

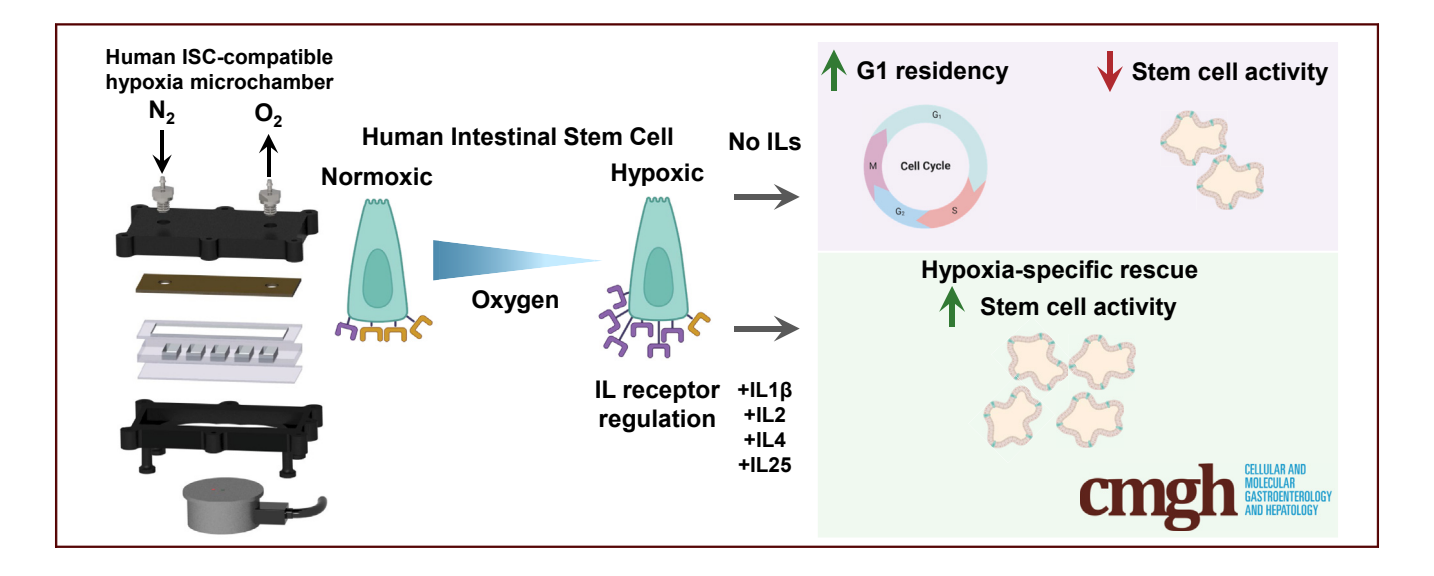
ORIGINAL RESEARCH

Hypoxia Primes Human ISCs for Interleukin-Dependent Rescue of Stem Cell Activity



Kristina R. Rivera, ^{1,*} R. Jarrett Bliton, ^{1,*} Joseph Burclaff, ¹ Michael J. Czerwinski, ² Jintong Liu, ² Jessica M. Trueblood, ³ Caroline M. Hinesley, ³ Keith A. Breau, ² Halston E. Deal, ¹ Shlok Joshi, ² Vladimir A. Pozdin, ⁴ Ming Yao, ⁵ Amanda L. Ziegler, ⁶ Anthony T. Blikslager, ⁶ Michael A. Daniele, ^{1,4} and Scott T. Magness ^{1,2,3,7}

¹Joint Department of Biomedical Engineering, North Carolina State University and University of North Carolina at Chapel Hill, Raleigh, North Carolina; ²Department of Cell Biology and Physiology, University of North Carolina at Chapel Hill, Chapel Hill, North Carolina; ³Center for Gastrointestinal Biology and Disease, University of North Carolina at Chapel Hill, Chapel Hill, North Carolina; ⁴Department of Electrical and Computer Engineering, North Carolina State University, Raleigh, North Carolina; ⁵Department of Mechanical and Aerospace Engineering, North Carolina State University, Raleigh, North Carolina; ⁶Comparative Medicine Institute, Department of Clinical Sciences, College of Veterinary Medicine, North Carolina State University, Raleigh, North Carolina; and ⁷Department of Medicine, University of North Carolina at Chapel Hill, Chapel Hill, North Carolina



SUMMARY

A new microphysiological system allows precise control and monitoring of oxygen levels at the cell surface to study the impact of hypoxia. Hypoxia pushes human intestinal stem cells (hISCs) into a dormant but reversible proliferative state and primes hISCs to respond to a subset of interleukins that rescues hISC activity.

BACKGROUND AND AIMS: Hypoxia in the intestinal epithelium can be caused by acute ischemic events or chronic inflammation in which immune cell infiltration produces inflammatory hypoxia starving the mucosa of oxygen. The epithelium has the capacity to regenerate after some ischemic and inflammatory conditions suggesting that intestinal stem cells (ISCs) are highly tolerant to acute and chronic hypoxia; however, the impact of hypoxia on human ISC (hISC) function has not been reported. Here we present a new microphysiological system (MPS) to investigate how hypoxia affects

hISCs from healthy donors and test the hypothesis that prolonged hypoxia modulates how hISCs respond to inflammation-associated interleukins (ILs).

METHODS: hISCs were exposed to <1.0% oxygen in the MPS for 6, 24, 48, and 72 hours. Viability, hypoxia-inducible factor 1a (HIF1a) response, transcriptomics, cell cycle dynamics, and response to cytokines were evaluated in hISCs under hypoxia. HIF stabilizers and inhibitors were screened to evaluate HIF-dependent responses.

RESULTS: The MPS enables precise, real-time control and monitoring of oxygen levels at the cell surface. Under hypoxia, hISCs maintain viability until 72 hours and exhibit peak HIF1a at 24 hours. hISC activity was reduced at 24 hours but recovered at 48 hours. Hypoxia induced increases in the proportion of hISCs in G1 and expression changes in 16 IL receptors. Prolyl hydroxylase inhibition failed to reproduce hypoxia-dependent IL-receptor expression patterns. hISC activity increased when treated IL1 β , IL2, IL4, IL6, IL10, IL13, and IL25 and rescued hISC activity caused by 24 hours of hypoxia.

CONCLUSIONS: Hypoxia pushes hISCs into a dormant but reversible proliferative state and primes hISCs to respond to a subset of ILs that preserves hISC activity. These findings have important implications for understanding intestinal epithelial regeneration mechanisms caused by inflammatory hypoxia. (Cell Mol Gastroenterol Hepatol 2023;16:823–846; https://doi.org/10.1016/j.jcmgh.2023.07.012)

Keywords: Inflammatory Hypoxia; Microphysiological System; Intestinal Stem Cells; Stem Cell Priming; Oxygen Sensor; Cytokines.

ellular respiration in complex multilayered tissues relies on a constant supply of oxygen to maintain healthy physiologic states. To this end, the intestinal epithelium maintains physiologic oxygen tension through a highly vascularized tissue that is perfused by a vast network of vessels that terminate in capillary beds where oxygen is released to adjacent cells in a local microenvironment. In the crypt-villus epithelial architecture, cells can experience marked differences in physiologic oxygen concentrations where crypt-based cells experience higher oxygen levels compared with cells at the villus tips. Along the crypt-villus axis, a steep oxygen gradient is present in which microenvironments that are separated by just ~ 100 cell distances experience a ~ 10 -fold lower oxygen concentration.³ While lower oxygen concentrations within the gradient are tolerated as normal, sudden or dramatic changes in the magnitude and duration of oxygen loss can lead to pathological hypoxia resulting in cell dysfunction or death.⁴

Most studies that evaluate the impact of tissue oxygen deprivation do so in the context of ischemia-reperfusion injury. This is characterized by an initial ischemic event such as bowel strangulation, aneurysm, or organ harvest for transplantation, which induces hypoxia. Subsequent reperfusion of blood flow, and thus oxygen, induces a separate type of oxidative injury caused by free radicals and reactive oxygen species.^{5,6} Hypoxic events can be categorized as acute, which are typically transient events that last on the order of minutes to hours, and chronic hypoxic events that last much longer, for at least 24 hours or more. Inflammatory hypoxia, a type of chronic hypoxia, is caused by the presence of large numbers of immune cells in the submucosal compartment depleting local oxygen supplies. 4,8,9 Following epithelial injury, a massive influx of immune cells is recruited to prevent pathogens and other luminal contents from causing further damage. This massive influx of immune cells consumes the local oxygen supply to the epithelium^{4,10-13} and can cause vasoconstriction, which further starves the epithelial cells of oxygen. 3,14,15 Hypoxia due to inflammation can exist in isolated microenvironments that might initially go unnoticed and eventually resolve themselves. However, longer periods of inflammation, such as in inflammatory bowel disease, may compromise the epithelium and normal repair mechanisms ultimately resulting in, or contributing to, mucosal erosions and ulcerations.^{8,12} Consistent with this concept, inflammatory responses have been shown to produce localized

and chronic hypoxic episodes in the intestinal stem cell (ISC) zone, potentially leading to impaired ISC survival, renewal, and differentiation, ultimately impeding mucosal repair and producing ISC death.^{6,15,16}

While numerous studies focus on the impact of hypoxia on repair mechanisms involving restitution in differentiated entrocytes, 6,17-21 few studies investigate the impact of hypoxia on ISC properties and ISC-dependent repair mechanisms, 22 especially in human tissues. Traditionally, human cancer cell lines are used to study acute and chronic hypoxia at the cellular level, but transformed cells exhibit abnormal proliferation and cell death dynamics and they do not properly differentiate; thus, they are poor models of human ISCs (hISCs).²³ Studies in porcine small intestines show that the so-called reserve ISC exhibits high tolerance to hypoxic episodes of up to 4 hours of hypoxia/ischemia, 15,22 but these studies do not evaluate the impact of chronic hypoxia on hISCs. A highly physiologically relevant human model to study acute ischemia was developed,²⁴ and while the study primarily characterizes the differentiated epithelium under hypoxia, a lack of apoptosis in the crypt observed after 45 minutes of ischemia indicates that hISCs are highly resistant to short hypoxic episodes.²⁰ Despite the important observations and advances outlined in these in vivo studies, all have been performed either in the context of ischemia-reperfusion injury, precluding the evaluation of hypoxic injury uncoupled from reperfusion injury, or performed under short-duration ischemic conditions (<4 hours), and thus interpretations are limited to acute rather than chronic hypoxia injury.

Investigating the impact of hypoxia on hISCs has been historically limited by the inability to indefinitely culture hISCs, the lack of high-resolution in vitro platforms in which oxygen levels can be tuned and accurately monitored in real time, and ethical considerations of human research that preclude in vivo experimentation. In this study, we engineered a microphysiological system (MPS) that delivers multiple durations and magnitudes of hypoxia to primary hISCs. The MPS allows for precise remote monitoring and control of oxygen concentrations in real-time at the cell surface interface. We use the MPS to create controlled durations of acute and chronic hypoxic episodes and evaluate dynamic transcriptomic changes within hISCs under these

*Authors share co-first authorship

Abbreviations used in this paper: 2D, 2-dimensional; 3D, 3-dimensional; CRA, CellRaft Array; DMOG, dimethyloxalylglycine; DPBS, Dulbecco's phosphate-buffered saline; EM, expansion media; FACS, fluorescence-activated cell sorting; GSEA, gene set enrichment analysis; HIF, hypoxia-inducible factor; hISC, human intestinal stem cell; IL, interleukin; iPOB, integrated phosphorescent oxygen biosensor; ISC, intestinal stem cell; MPS, microphysiological system; NF- κ B, nuclear factor κ B; NIR, near infrared; OFE, organoid forming efficiency; PBS, phosphate-buffered saline; PC, principal component; PCR, polymerase chain reaction; PHD, prolyl hydroxylase; PMMA, polymethylmethacrylate; qRT-PCR, quantitative real-time polymerase chain reaction.

Most current article

© 2023 The Authors. Published by Elsevier Inc. on behalf of the AGA Institute. This is an open access article under the CC BY-NC-ND license (http://creativecommons.org/licenses/by-nc-nd/4.0/).

2352-345X

https://doi.org/10.1016/j.jcmgh.2023.07.012

conditions. We focused our evaluation on chronic hypoxic events related to hISC-immune cell crosstalk through interleukin (IL) signaling that might occur during inflammatory hypoxia. Our findings have broad implications for understanding the role in which inflammatory hypoxia can impact hISC behavior in gross clinical presentation of ischemia-reperfusion injury and focal ischemic events that occur in inflammatory bowel disease-related hypoxia.

Results

A New Microscopy-Compatible MPS Enables Precise Regulation and Real-Time Monitoring of Oxygen Levels at the Cell-Media Interface

To address the limitations of sensitivity, accuracy, and scale in existing environmental culture systems that create a hypoxic environment, we developed a novel MPS the size of a standard microscope slide where oxygen tension could be tailored to precise levels. The MPS design consists of 2 major structural components: (1) the 3-dimensional (3D)-printed light- and air-tight container required for phosphorescence detection and hypoxia induction in the closed system and (2) a clear-bottomed acrylic 5-well tissue culture plate with each well containing a hydrogel scaffold that facilitates hISC expansion, which all sits inside of the sealed chamber (Figure 1A and B, see Materials and Methods).²⁵

The MPS was designed as a closed system in which ambient air flowed over each well via continuous delivery of mixed gases. A biocompatible integrated phosphorescent oxygen biosensor (iPOB) was placed on the hydrogel scaffold surface to provide real-time oxygen measurements specifically at the cell surface interface (Figure 1*C*).²⁶ Oxygen levels were quantified by the iPOB using near infrared (NIR) phosphorescence lifetime fluorimetry, which measures the oxygendependent decrease in phosphorescence lifetime to determine local oxygen concentration (Figure 1*C* and *D*).²⁷ The iPOBs are reusable, highly sensitive, and capable of detecting a broad range of oxygen levels created by an off-chip gas mixer28 (Figure 1*D*, see Materials and Methods).

The MPS design facilitates easy access to refresh media, add compounds, and perform a variety of downstream assays including microscopy, transcriptomic analysis, and immunostaining. The device is fabricated from relatively inexpensive commercially available materials and can be sterilized and reused many times. Notably, multiple MPSs can be connected to the same gas source to accommodate complex experimental designs that require many perturbations and technical replicates (see Materials and Methods). Together, these demonstrate an ideal model system for evaluating the effect of hypoxia on hISCs.

The MPS Supports Culture of hISC/Progenitor Epithelial Monolayers

We recently developed methods that support indefinite 2-dimensional (2D) expansion of proliferative human ISCs from primary small intestine and colon. Under normoxic conditions (ie, 37° C, 5% CO₂, and remainder atmospheric air), hISC monolayers can be cultured on a defined hydrogel

and media formulation that supports hISC expansion while repressing differentiation. ^{25,28} This method was used to expand primary jejunal hISCs isolated from small intestinal crypts of an organ transplant donor and then transferred to the MPS. Initial characterization of the proliferative hISC monolayer was performed in the MPS under normoxic conditions by immunostaining. The monolayers demonstrated DNA synthesis as measured by S-phase marker EdU, expression of hISC/progenitor cell marker SOX9, ^{29,30} and epithelial cell tight junction protein occludin (Figure 1E). These results demonstrate the MPS is biocompatible with primary hISCs that are consistent with proliferating hISC/progenitor cell populations.

Next, the baseline functional stemness of proliferative hISCs cultured on the MPS under normoxia was evaluated. hISCs were cultured on the MPS as proliferative monolayers under atmospheric O2 levels, dissociated to single cells and plated in Matrigel on a CellRaft Array (CRA) to assess organoid forming efficiency (OFE), a measure for in vivo hISC activity. 31-33 Single cells in the microwells were identified and quantified, and putative hISCs were individually tracked over a 6-day culture period to determine whether an organoid formed. The data demonstrate $\sim 4\%$ of single cells cultured in the MPS under hISC expansion conditions generated an organoid at each time point measured (2, 4, and 6 days after plating) (Figure 1F), which is consistent with OFE of fluorescence-activated cell sorting (FACS)-isolated hISCs from a Lgr5-EGFP expressing reporter gene mouse and also consistent with human organoid-derived hISCs cultured for the same period of time in synthetic matrices.^{33,34} These findings demonstrate that hISCs cultured as 2D monolayers on the MPS maintain hISC properties over time, and at similar ratios to those observed in vivo and in 3D organoid systems.

To define the speed at which severe hypoxia could be achieved and maintained in the MPS, an iPOB was added to the epithelial cell surface, and real-time oxygen levels at the cell-media interface were measured for 24 hours (Figure 1G, inset). Oxygen concentrations of <1% (below 10 μ M) are considered severely hypoxic but not anoxic. 35 The data show that the MPS produced a rapid hypoxic environment of 0.3% O_2 (3 μ M) within ~30 minutes, which was constantly maintained during the 24-hour experiment (Figure 16). Interestingly, when proliferative hISC monolayers were cultured in normoxic conditions as a control, cellular respiration reduced oxygen levels at the cell-media interface from 18% (180 μ M) to 3.5% (35 μ M) in the MPS. These data demonstrate that physiologic O2 metabolism of proliferative hISCs produce a steady-state flux of O2 in just 30-minutes that is 5-fold less than atmospheric oxygen levels.

Human ISC Monolayer Cultures Demonstrate Peak Hypoxia-Inducible Factor 1a Response at 24 Hours of Severe Hypoxia With No Loss of Stem Cell Activity After 48 Hours of Severe Hypoxia

The hypoxia-inducible factor 1 (HIF1) transcription factor¹³ is a master regulator of the hypoxic response

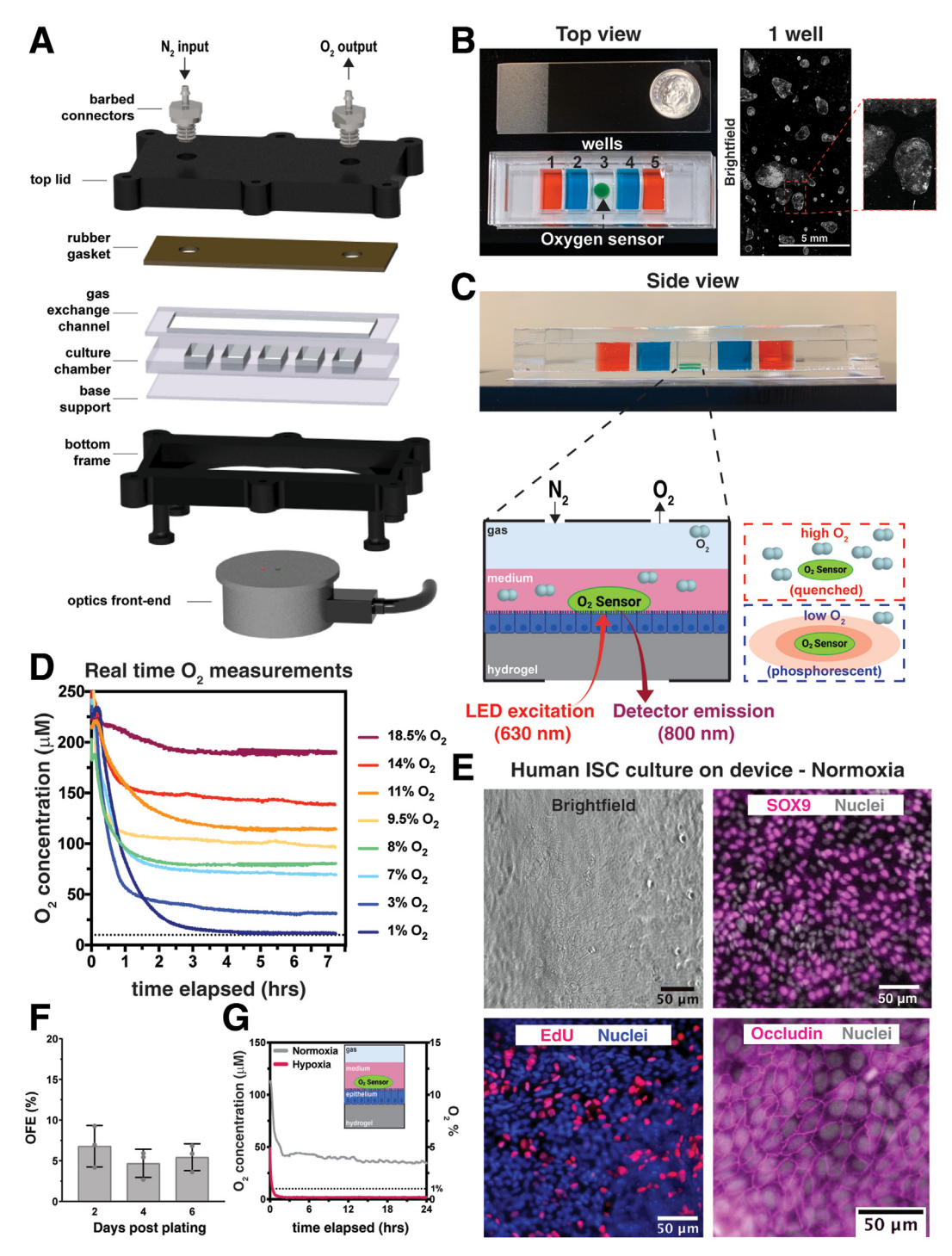


Figure 1. Development of a tunable hypoxic MPS with integrated oxygen sensors and cultured primary human intestinal epithelium. (A) Exploded view of MPS compartments. (B) (Left) Top view photograph of a standard microscope glass slide (75 × 25 mm) and dime, for reference, placed above the MPS with iPOB (black arrow) inside well 3 and red and blue dyes in wells 1 and 5 and 2 and 4, respectively. (Middle) 1 well brightfield image of monolayer of cells. (Right) Inset from 1 well brightfield image shows magnified colonies in the hISC monolayer. (C) (Top) Side-view photograph of MPS with middle well containing the green iPOB. Schematic of iPOB integrated into hydrogel to measure oxygen at the cell layer inside the cell culture well. (Bottom left) Schematic of porphyrin-based luminescence. In high oxygen, luminescence from the porphyrin is quenched by energy transfer to oxygen, resulting in a decrease in phosphorescence lifetime. In the absence of oxygen, porphyrin molecules are excited by LED from the detector and phosphoresce with increased lifetime. (D) Plots of 8 oxygen concentration vs time (7.5 hours) measurements from the iPOB inside the MPS, with 8 different mixed gas inputs, show generation of 8 established oxygen environments. (E) (Top left) Brightfield image of human intestinal epithelial stem and progenitor cells grown inside an MPS well to confluence. Fluorescent images show tight junction structures between epithelial cells marked by the protein occludin (magenta, bottom right), stem cells marked by SOX9 (magenta, top right, and proliferative cells marked by EdU (red, bottom). Nuclei are marked by Bisbenzimide+ staining in gray or blue. (F) OFE (%) measured over 6 days from single cells isolated from MPS after 5 days in culture. (G) Oxygen concentration tracked using the iPOB inside an MPS containing human intestinal epithelium for 24 hours with normoxic and hypoxic culture environments.

conserved across all tissues and species. 14,36 Under normoxia, HIF1a is constitutively expressed but is immediately targeted for degradation.14 By contrast, under hypoxia, HIF1a degradation is inhibited through well-established mechanisms. The rapid accumulation of HIF1a binds $HIF1\beta$ to complete the HIF1 transcription factor resulting in the regulation of a broad range of downstream target genes that regulate cell survival, proliferation, metabolism, and cell migration. 13,37 Immunostaining for HIF1a in hISCs under durations of hypoxia shows a significant accumulation of HIF1a only at 24 hours of severe hypoxia (Figure 2A and B). No significant change in HIF1a was observed at 6 hours of hypoxia compared with normoxia, which may indicate tolerance of proliferative hISCs to shorter hypoxic episodes. Lack of HIF1a accumulation at 48 hours of hypoxia is likely due to known dampening of the HIF response that occurs after cells re-equilibrate to tolerate new and sustained low O2 levels. Interestingly, hISCs cultured under normoxia showed a significant increase in HIF1a levels 24 hours after media change when compared with the 6-hour normoxic samples. This minor hypoxic response is consistent with previous observations that cells in submersion cultures experience a localized hypoxic environment due to the slower rate of diffusion of O2 through medium relative to the rate of consumption in cellular metabolism.³⁸ Together, these findings established a time frame for further investigation into the mechanisms by which hISCs resist death and preserve functional stemness and viability in response to HIF1a accumulation in hISCs during short-, medium-, and long-term hypoxia.

To confirm whether proliferative hISCs in the MPS were experiencing a HIF response at 0.3% O2, quantitative polymerase chain reaction (PCR) was performed to detect expression of canonical HIF-1 target genes that are typically upregulated during hypoxia. While HIF-1 activity is primarily regulated by posttranscriptional mechanisms, 39,40 hypoxia induced a significant reduction in HIF1A expression across all timepoints (6 hours = 2.7-fold, 24 hours =1.2-fold, 48 hours = 4.9-fold) (Figure 2C). There was a robust transcriptional response of classic HIF1 target genes, VEGFA, SCL2A1/GLUT1, and BNIP3, as early as 6 hours of hypoxia and the upregulation of these genes persisted through 24 hours of hypoxia (Figure 2C). 41-43 At 48 hours of hypoxia, SCL2A1/GLUT1 and BNIP3 remained upregulated but interestingly VEGFA returned to normoxic levels (Figure 2C) suggesting that HIF-independent mechanisms regulate VEGFA expression after 48 hours of hypoxia. These results demonstrate that exposure to an O₂ tension of 0.3% (3 μ M) activates a canonical hypoxia response in hISCs.

Next, we sought to explore the extent to which hISCs can survive severe hypoxia. hISCs were exposed to severe hypoxia (<1% O_2 as measured by the iPOB) in the MPS for 6, 24, 48, or 72 hours and viability was evaluated by staining for early apoptosis marker, Annexin V (Figure 2D). How cytometric quantification of Annexin V-negative cells shows $\sim 90\%$ viability through 48 hours of severe hypoxia. However, at 72 hours of severe hypoxia, there was a significant decrease in viability as measured by Annexin V-negative staining, from $\sim 90\%$ viable in normoxic controls to $\sim 70\%$ viable after 72 hours of hypoxia.

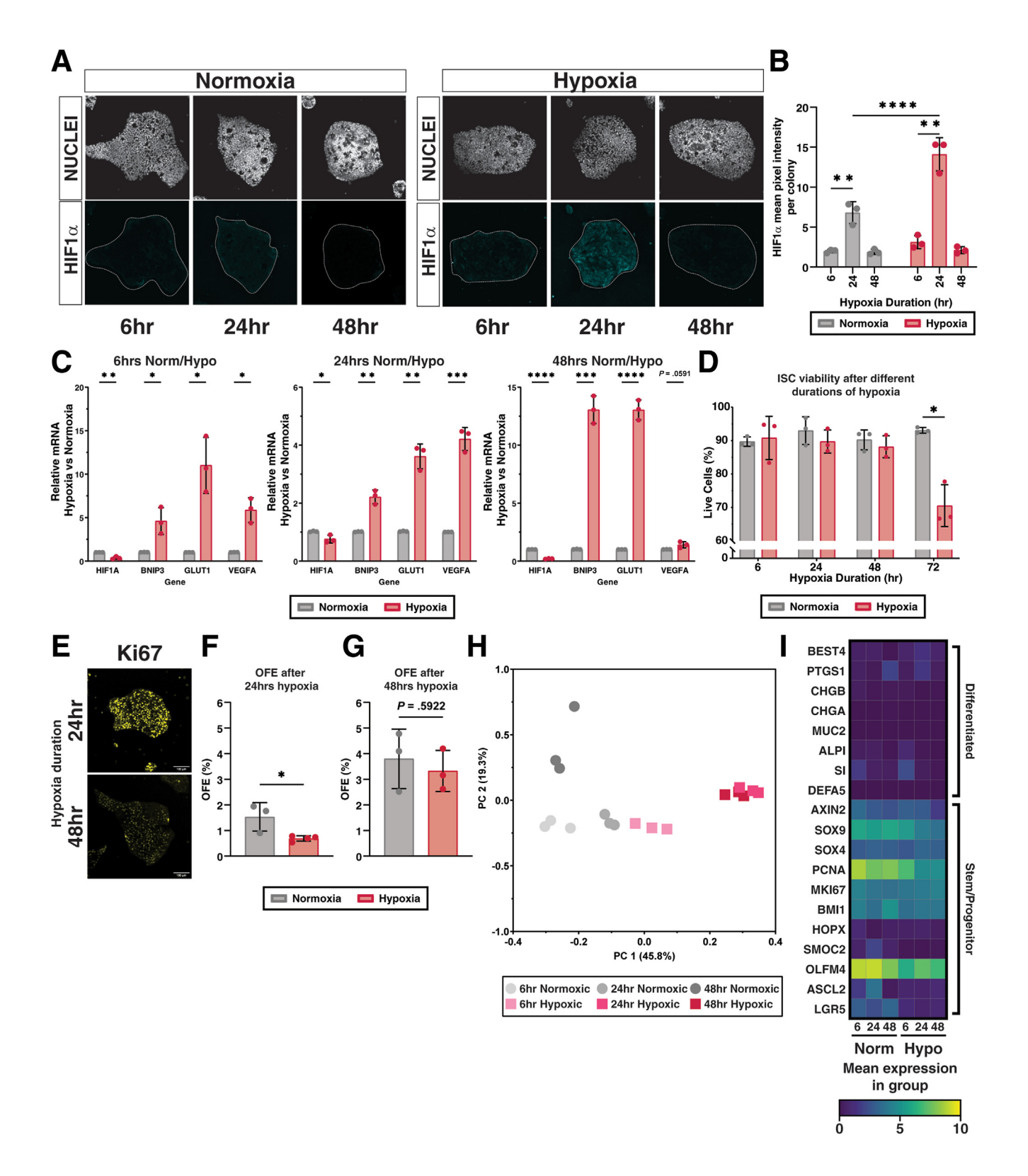
To determine how longer episodes of hypoxia would impact hISC activity, monolayers were exposed to 24 hours or 48 hours of hypoxia or normoxia as a control in the MPS. At 24 and 48 hours of hypoxia, hISCs demonstrate persistent expression of the proliferation marker, KI67, albeit nuclear KI67 levels are reduced at 48 hours of hypoxia (Figure 2E). To quantify hISC activity after these durations of hypoxia, monolayers were subjected to 24 or 48 hours of hypoxia, dissociated to single cells, and then applied to CRAs for high-throughput accurate quantification of clonal OFE.33 CRAs enable up to $\sim 10,000$ hISCs to be plated in microwells on a small device and individual hISCs can be evaluated for OFE over time. 33,45 After 24 hours of hypoxia, OFE decreased ~ 2.5 -fold (Figure 2F). Interestingly, when hISCs were exposed to a longer 48-hour hypoxia duration, the OFE was indistinguishable from normoxia controls, suggesting that hypoxia-induced survival mechanisms were invoked in hISCs after 24 hours of hypoxia (Figure 2G).

To evaluate the time-dependent gene expression changes occurring in response to hypoxia and HIF1a accumulation, RNA sequencing was performed on proliferative hISCs cultured under normoxia and severe hypoxia for 6, 24, and 48 hours (Figure 2H). Principal component (PC) analysis demonstrated high agreement between technical replicates (n = 3) for each timepoint and revealed global transcriptomic changes in hISCs between normoxic and hypoxic samples. The 6- and 48-hour normoxic samples clustered closely on the first PC, whereas the 24-hour normoxic samples deviated from the other normoxic samples on the first PC. Interestingly, the 48-hour normoxic samples deviated from the 6-hour normoxic samples on the second axis, which is consistent with our previous data that hISCs mount a transient HIF response at 24 hours following media change that resolves after 48 hours in culture (Figure 2A and B). These results suggest that normoxic hISCs experience a minor hypoxic event following media change that results in a subtle, but meaningful, shift in gene expression profile in line with a hypoxic response and that following this shift, the hISCs return to a slightly altered gene expression profile.

For hypoxic samples, the 6-hour samples clustered closest to the 24-hour normoxic samples, which is consistent with the previous observation that the 24-hour normoxic hISCs were undergoing a minor HIF response. By contrast, the 24- and 48-hour hypoxic samples clustered together but deviated significantly from all other samples on the first PC, suggesting the onset of a strong HIF response in hISCs at 24 hours of severe hypoxia that persists through 48 hours of hypoxia. The transcriptomic shift at 24 hours of hypoxia is aligned with the robust HIF1a accumulation and significant decrease in OFE after 24 hours of hypoxia, reinforcing the concept that hISCs tolerate shorter periods of hypoxia through at least 6 hours but require transcriptional changes at 24 hours to regain organoid forming activity at 48 hours (Figure 2F and G).

To determine if durations of severe hypoxia promoted differentiation, transcriptomic analysis was performed to evaluate the expression of hallmark lineage markers for hISCs and main classes of differentiated cells (Figure 21). 46,47 Consistent with decreased OFE at 24 hours of hypoxia, hISCs show decreased expression of stem and progenitor marker genes. Interestingly, this decreased expression continues through 48 hours of hypoxia, even

though OFE is restored to normoxic levels, which is consistent with the changes seen in our PC analysis (Figure 2H). The data show very low expression and no appreciable trends in hypoxia-associated changes of genetic



markers for absorptive enterocytes (ALPI, SI) and secretory lineages, Paneth (DEFA5), enteroendocrine (CHGA, CHGB), tuft (PTGS1), Goblet (MUC2), and BEST4 cells (BEST4) compared with markers of proliferative hISCs and progenitor cells. These data indicate that hypoxia alone does not promote differentiation of hISCs.

Hypoxia Primes an hISC Transcriptional State to Respond to Extrinsic IL Signals and Intrinsic Downstream Mediators of Inflammation

Gene set enrichment analysis (GSEA) was used to investigate the potential molecular and physiological processes associated with the time-dependent transcriptomic changes. GSEA demonstrates that the hallmark hypoxia gene set peaks at 24 hours but is highly enriched at all timepoints providing in the pathway-based analysis (Figure 3A). 48,49 Twenty-eight of the top significantly regulated gene sets demonstrated consistency with known hypoxiaassociated processes such as glycolysis, angiogenesis, and the unfolded protein response.^{50–52} A notable set of processes emerged that were related to inflammation including the GSEA terms inflammatory response, IL6 JAK STAT3 signaling, IL2 STAT5 signaling, and INFa/g responses (Figure 3A).

Within the gene set for hallmark inflammatory response, \sim 4.5% (n = 8 of 184) of the genes were IL receptors and all demonstrated some form of hypoxia-dependent regulation; thus, we focused our analysis on all IL receptors 4,10,14 with the goal of revealing how hypoxia-related inflammatory conditions might extrinsically signal to hISCs (Figure 3B). ILs and their cognate receptors have well established roles in regulating stem cell proliferation in diverse tissue types.⁵³⁻⁶² Of 45 IL receptors, 91% had detectable expression across all durations of hypoxia. Differential gene expression between normoxic and hypoxic environments revealed a subset of 13 IL receptors (IL1R1, IL1R2, IL1RAP, IL1RAPL1, IL2RG, IL4R, IL11RA, IL13RA1, IL17RA, IL17RC, IL17RE, IL18R1, IL20RA) that were regulated by hypoxia in a time-dependent fashion, potentially indicating specific roles during early (6 hours), mid (24 hours), and late (48 hours) durations of severe hypoxia.

To compare hypoxia-dependent changes in IL receptor expression, we looked at differences in gene expression for

the 45 IL receptor genes observed in our dataset. IL1RAPL1, IL1R2, IL10RB, IL22RA1, IL6R, IL11RA, IL17RE, IL1RN, IL2RG, IL4R, IL17RA, and IL17RB were considered early responders, as all showed hypoxia-dependent up- or downregulated expression at 6 hours (Figure 4A). Of the early responders, IL1RN, IL6R, IL10RB, IL17RB, and IL22RA1 were considered early persistent responders as their hypoxia-dependent expression changes were consistent through 24 and 48 hours of hypoxia (Figure 4A-C). IL1RAP, IL1R1, IL18R1, and IL20RA were considered mid responders, as their regulation patterns changed beginning at 24 hours of hypoxia. Of these, only IL1RAP had significant change in regulation through 48 hours. IL13RA1 and IL17RC were considered late responders, as their hypoxiadependent gene expression patterns were only observed following 48 hours of hypoxia. IL1R2 and IL11RA were considered dynamic responders, as their expression patterns changed at 6 and 48 hours of hypoxia. The significant trends were verified by quantitative PCR for the subset of IL receptors that were consistently upregulated (IL6R, IL10RB, IL22RA1) or downregulated (IL17RB) (Figure 4D). To confirm that hISCs expressed the IL receptors in vivo and in the MPS culture system, we compared IL receptor expression from our recent single cell transcriptomic atlas of the human intestine to single-cell transcriptomic dataset for hISCs cultured as monolayers in media that supports hISC expansion (Figure 4E and F). 47,63 The data show that all members of the subset of hypoxia-regulated IL receptors have measurable expression in hISCs both in vivo and in vitro. These results show hISC undergo time-dependent changes in IL receptor expression during acute and chronic hypoxic events that prime hISCs to respond to extrinsic inflammatory signals.

Prolyl Hydroxylase and HIF Inhibitor Screening Suggests That IL Receptor Expression Is Mediated by Alternative Hypoxia-Dependent Mechanisms

A number of small molecules have been designed to potentiate or inhibit HIF activity. We tested 2 compounds, Roxadustat and dimethyloxalylglycine (DMOG), which

Figure 2. (See previous page). Primary human intestinal epithelium cultured under hypoxia inside microphysiological system shows dynamic response to different durations of hypoxia. (A) Representative images of human intestinal stem cells colonies cultured on collagen scaffolds as 2D monolayers showing changes in HIF1a immunofluorescence staining over different durations of normoxia or hypoxia. (B) Quantification of mean pixel intensity of HIF1a staining in panel A. Technical replicates represent mean pixel intensities of all nuclei in 3 individual colonies. Mean pixel intensities across all conditions were compared with 1 way analysis of variance with Holm-Sídák's multiple comparisons test. (C) qRT-PCR results of human intestinal epithelium for downstream HIF1 targets (BNIP3, GLUT1, VEGFA) after 6, 24, and 48 hours of normoxic or hypoxic environment exposure. (D) Flow cytometry results from single cells isolated after 6, 24, 48, and 72 hours from normoxic and hypoxic MPS and stained for Annexin V(-) to quantify cell viability cells (%). Mean percentage of AnnexinV- cells from 3 normoxic and hypoxic samples were compared using unpaired t tests. (E) Immunostaining of hISC monolayer colonies for proliferation marker KI67 following 24 or 48 hours of hypoxia. (F) Functional stemness as measured by OFE for 24-hour normoxic and hypoxic samples after 6 days of 3D Matrigel-embedded culture. (G) Functional stemness for 48-hour normoxic and hypoxic samples after 6 days of 3D Matrigel-embedded culture. Mean OFEs were compared by using unpaired t tests. (H) PC analysis of RNA sequencing results showing clusters of replicate samples from each time point (6, 24, and 48 hours) and condition (normoxia or hypoxia). Bulk RNA sequencing samples were sequenced from a range of 39-93 million reads. (/) Heatmap showing mean counts per million (CPM)-normalized and log-transformed expression of stem/progenitor markers or differentiated lineage markers from hypoxia bulk RNA sequencing in panel 2H. *P < .05, **P < .005, ***P < .001, ****P < .0001.

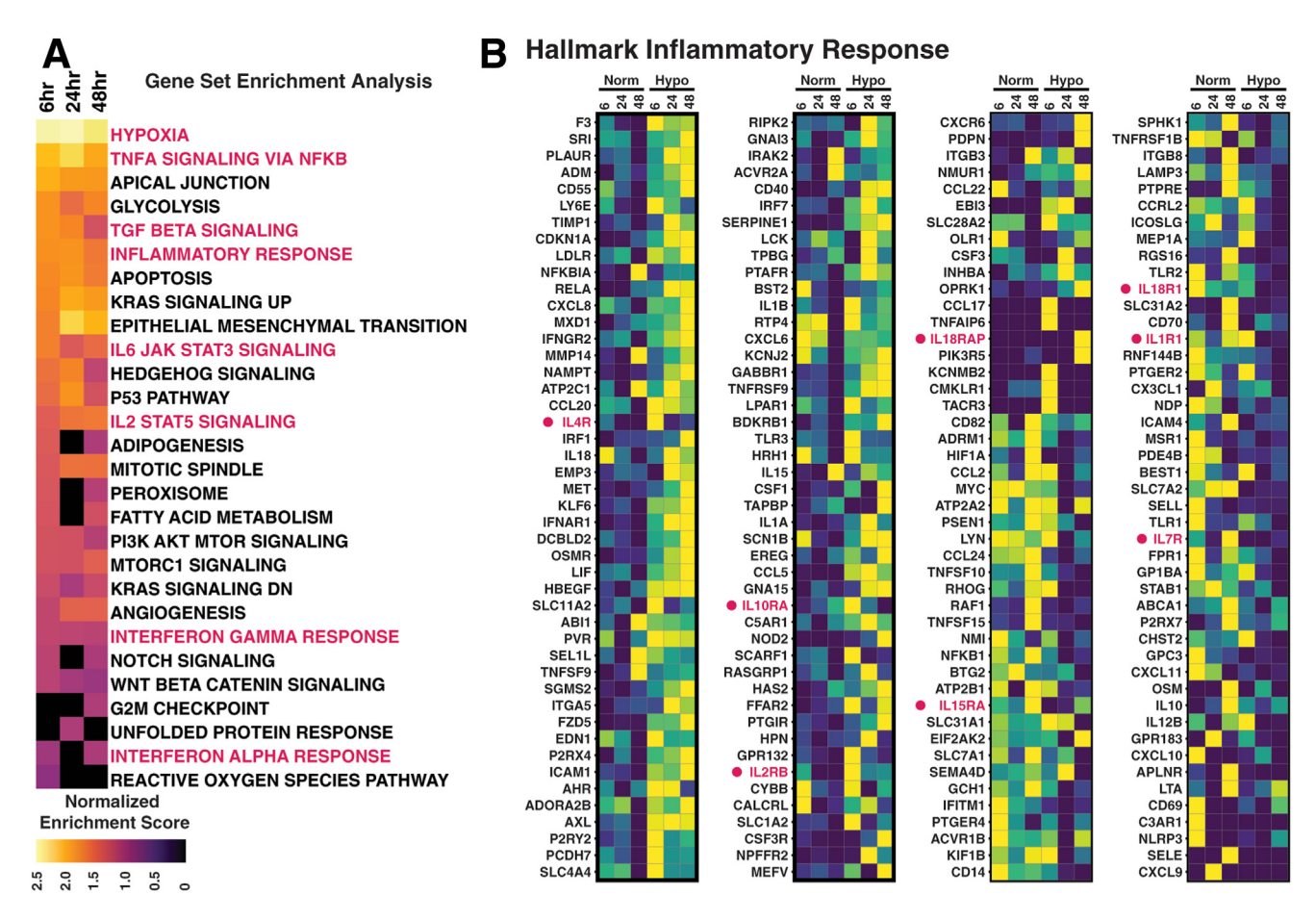


Figure 3. Characterizing the transcriptomic response to different durations of hypoxia by primary human intestinal epithelium. (A) Hallmark GSEA results for differentially expressed genes at each time point of hypoxia shown compared with normoxic controls. Differently expressed genes from RNA sequencing from each timepoint from Figure 2H were compared using GSEA and ranked by the normalized enrichment score. Gene sets related to hypoxia or inflammatory signaling are highlighted in pink. (B) Heatmaps of gene expression from bulk RNA sequencing data from Figure 2H for all genes from the hallmark inflammatory response GSEA gene expressed in the bulk dataset. IL receptors from the hallmark inflammatory response gene set that are expressed in our dataset are highlighted in pink.

inhibit prolyl hydroxylases (PHDs), the enzymes responsible for the constant degradation of HIF1a in normoxia.8,13 Inhibiting PHDs in normoxic hISCs should result in HIF1a accumulation and activation of its downstream target genes. When hISCs were cultured for 24 hours with Roxadustat. HIF1a target genes, BNIP3, GLUT1, and VEGFA, showed significant upregulation; however, DMOG treated hISCs showed no significant differences in HIF1a target genes (Figure 5A and B). Next, we sought to determine whether Roxadustat would upregulate IL receptors in primary hISC under normoxic conditions as observed under hypoxia. Following 24 hours of Roxadustat treatment under normoxia, only IL10RB was significantly upregulated, while the other IL receptors trended toward upregulation but did not reach significance (Figure 5C). These results indicate that pharmacological potentiation of HIF1a accumulation was not alone sufficient to recapitulate the magnitude of gene expression changes observed in hISCs under hypoxia for 24 hours, suggesting that other oxygen-dependent, HIF1a-independent pathways contribute to the full activation of IL receptor gene expression.

We next screened 2 HIF1a inhibitors, PX-478 and KC7F2, which both inhibit translation of HIF1a protein. 64,65 To determine whether the transcriptional changes mediated by hypoxia could be pharmacologically inhibited, hISCs were treated with the HIF1a inhibitors under hypoxia for 24 hours. The data show no significant impact on HIF1a target genes, BNIP3, GLUT1, and VEGFA, with PX-478 (Figure 5D). By contrast, KC7F2 treatment demonstrated a bimodal response where BNIP3 was significantly downregulated as might be expected, but GLUT1 and VEGFA were significantly upregulated (Figure 5*E*). These unexpected results highlight the importance of screening drugs in primary tissues, as both drugs have been shown to inhibit HIF1A primarily in cancer cell lines.^{66,67} While not the focus of this present study, specific HIF1a-dependent transcriptional regulation in hISC will require HIF1A knockout experiments.

Hypoxia Increases Proportion of hISCs Residing in G1 Phase

As a baseline, in the absence of ILs, we determined the impact of hypoxia on regulating proliferation and cell cycle

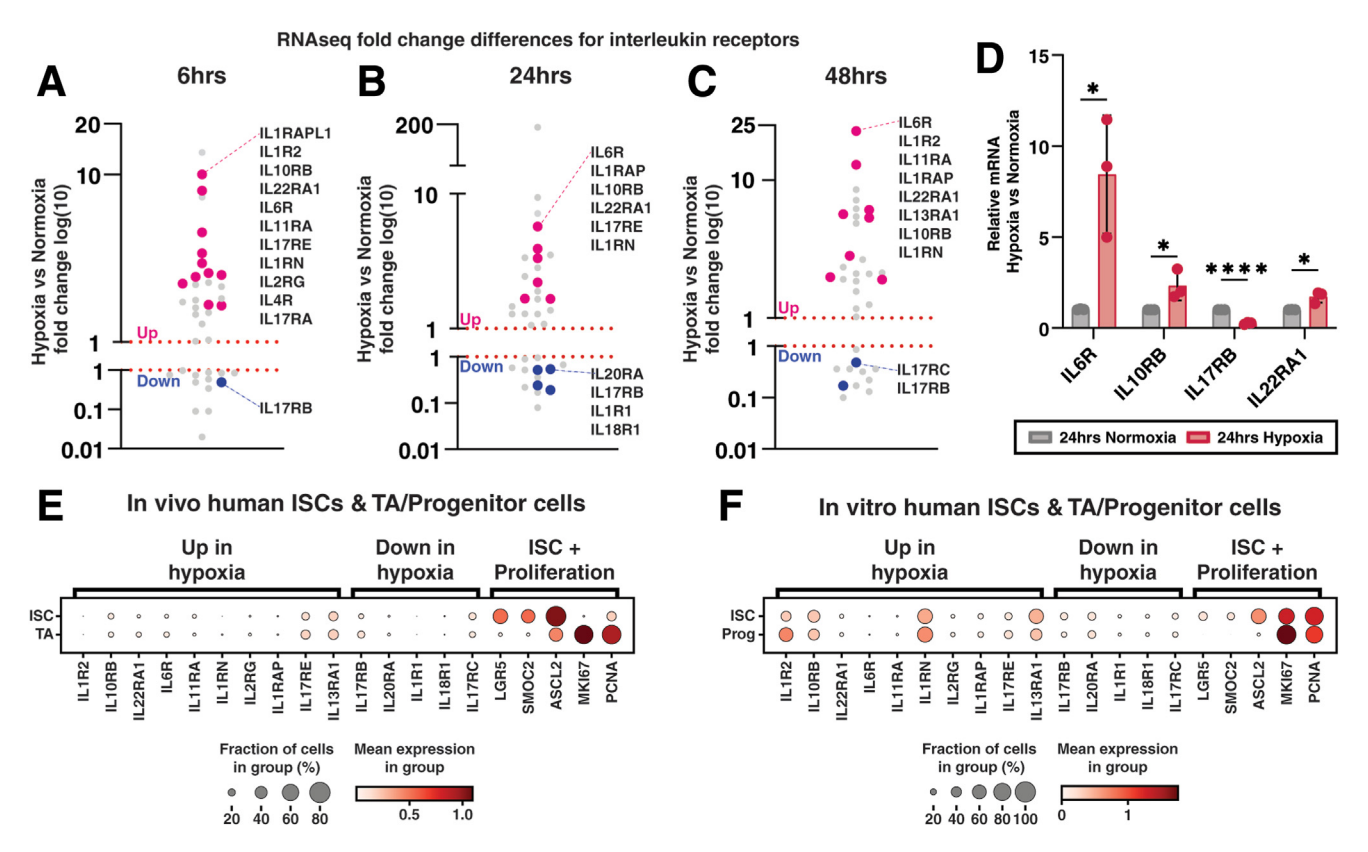


Figure 4. Hypoxia-induced changes in hISC gene expression for IL receptors. (*A–C*) Fold change comparison of expressed IL receptor genes from each duration of hypoxia in Figure 2*H* is shown. Differentially expressed genes that are upregulated in hypoxia compared with their normoxic counter parts are shown above 1 and genes downregulated in hypoxia are shown below 1. Pink dots signify genes that are significantly upregulated in hypoxia at a given time point and blue dots represent genes that are significantly downregulated in hypoxia at a given time point. Gray dots represent IL receptor genes that are not significantly differentially expressed at a given time point. Text lists genes represented by the colored dots sorted by descending fold change. (*D*) qRT-PCR measured after 24 hours of normoxia or hypoxia for IL receptor genes that are consistently up- or down-regulated at either 6, 24, or 48 hours of hypoxia. (*E*) Dot plot showing differentially expressed gene IL receptors from panels *A–C* and hISC and proliferation marker genes from hISC and Transit amplifying (TA) cells from single-cell RNA sequencing data of primary human intestinal epithelium. (*F*) Dot plot showing DEG IL receptors from panels *A–C* and hISC and proliferation marker genes from hISC and TA cells from single-cell RNA sequencing data of in vitro primary hISC and progenitors. **P* < .05, ******P* < .0001.

phases (Figure 6A). hISC monolayers were pulsed with EdU for the last 2 hours of culture to quantify cells in S-phase during normoxia or hypoxia, then costained for general cellcycle marker KI67 (Figure 6B). Individual nuclei were segmented using Cellpose and the percent of cells in S-phase (EdU⁺) or in any cell cycle phase (KI67⁺) were quantified. 68,69 Confocal images were used to train the algorithm for precise nuclear segmentation (Bisbenzimide+). Approximately 150,000 nuclei were automatically identified (ie, experimental all segmented) across conditions (Figure 6B). 68,69 After segmentation, KI67 and EdU channels were overlaid onto the automatically segmented nuclei to quantify the mean fluorescence intensity and percent of cells positive for each cell cycle marker on a per-nuclei and percolony basis. The number of cells in mitosis (M-phase) were evaluated by counting condensed chromosomes that were stained by KI67 and morphologically identifiable (Figure 6C).

To determine whether hypoxia caused a specific arrest or delay in any particular cell cycle phase, we leveraged a

recent study that shows that KI67 expression levels can reliably predict cell cycle phases. 70 KI67 levels can serve as a marker for cell cycle progression and exit, with the lowest levels of KI67 in G1/G0 phase, intermediate levels during Sphase, and highest levels in G2/M phase. 70 We evaluated the levels of KI67 in hISCs for segmented nuclei from ~38,000 cells and found that severe hypoxia significantly decreased KI67 under severe hypoxia (Figure 6D). Hypoxic hISC cultures showed approximately 67.2% of cells undergoing cell cycling (KI67⁺), a significant decrease compared with normoxic conditions in which 78.9% of cells reside in the cell cycle (Figure 6E).⁷⁰ More granular analysis revealed reductions in the number of cells in S-phase (EdU+) and Mphase (mitotic bodies) (Figure 6E). The lower levels of KI67, combined with the significant decrease in S- and M-phase cells, suggest that 24 hours of severe hypoxia likely causes either G1 arrest or lengthening of G1. Transcriptomic data do not show increases in differentiated lineage markers (Figure 21), indicating that hypoxia is not pushing hISCs to

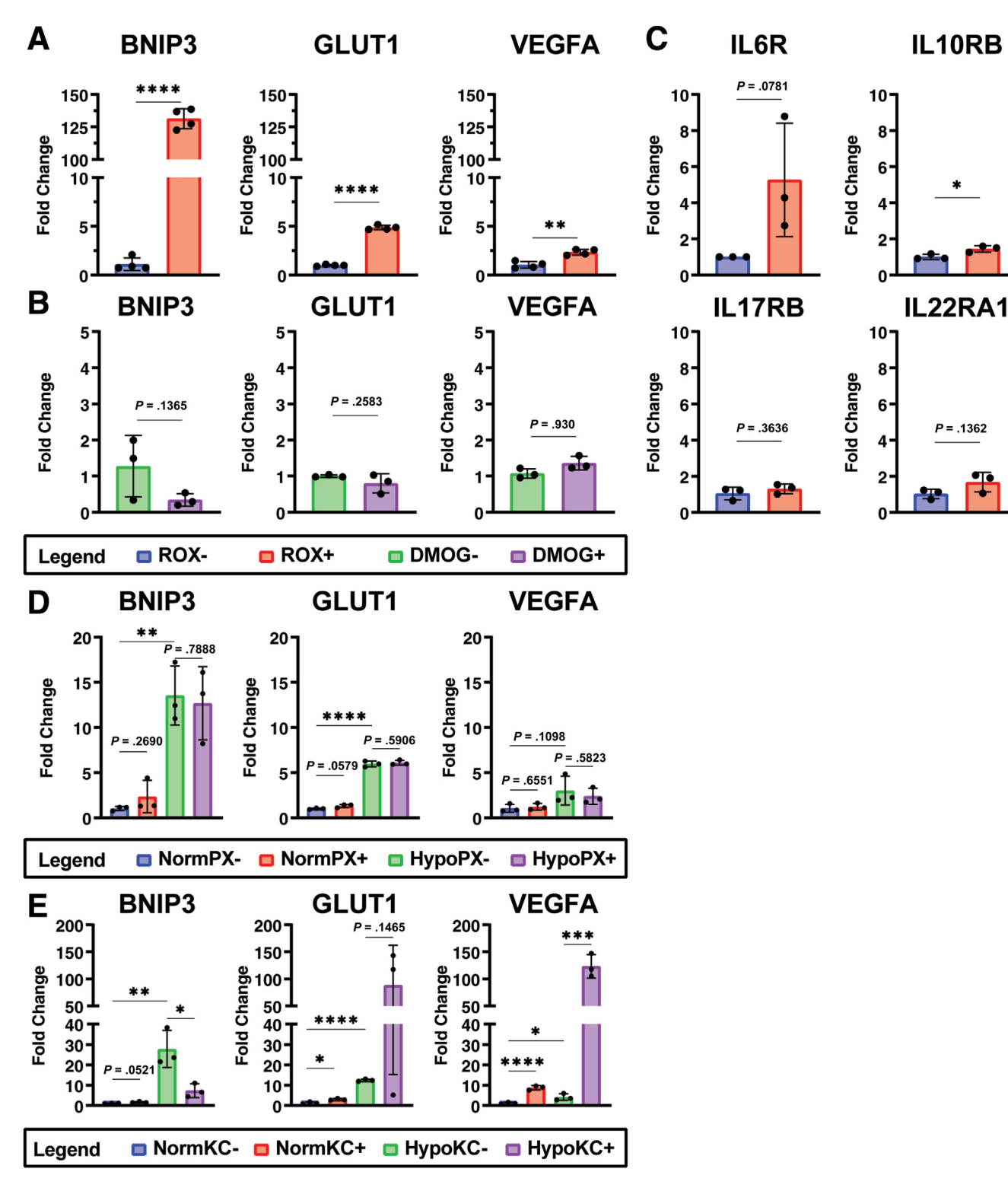


Figure 5. Screening PHD and HIF inhibitors on hISCs. (A) qRT-PCR for HIF1 target genes measured after 24 hours of normoxia and treatment with PHD inhibitors Roxadustat or DMOG. (B) qRT-PCR for IL receptor genes measured after 24 hours of normoxia and Roxadustat treatment. (C) qRT-PCR for HIF1 target genes measured after 24 hours of normoxia or hypoxia and vehicle or HIF inhibitor PX-478 treatment. (D) qRT-PCR for HIF1 target genes measured after 24 hours of normoxia or hypoxia and vehicle or HIF inhibitor KC7F2 treatment. *P < .05, **P < .005, ***P < .001, *****P < .0001.

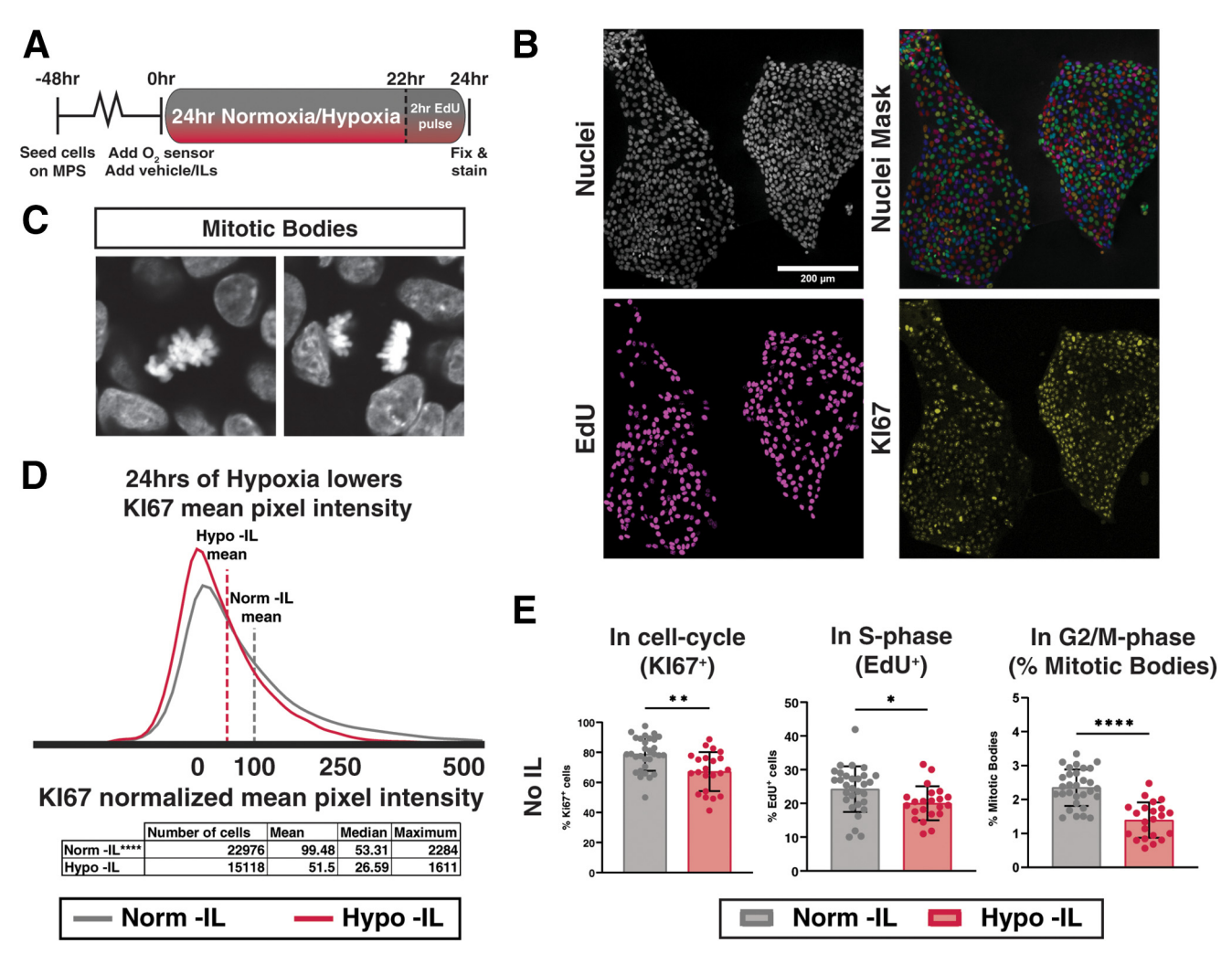


Figure 6. Severe hypoxia increases proportion of hISCs residing in G1 phase. (A) Experimental schematic to assess impact of hypoxia and ILs on cell cycle progression in human intestinal epithelial cells. (B) Example of raw confocal imaging data showing Bisbenzimide+ nuclei (top left), Cellpose-segmented nuclei mask, (top right), EdU (bottom left), and KI67 (bottom right). (C) Example of mitotic bodies found in KI67 channel. (D) Histogram showing distribution of normalized KI67 mean pixel intensities across normoxic and hypoxic conditions without IL treatments. The table shows key descriptive statistics that highlight statistically significant differences in distributions. ****P < .0001 by Kolmogorov-Smirnov test of cumulative distributions. (E) Percent of KI67+, EdU+, and mitotic bodies counted per colony in normoxic and hypoxic conditions without treatment from ILs and their comparison. Mean percentages for each marker were compared between normoxic and hypoxic conditions using unpaired t tests. Dots represent per-colony averages of single-cell mean pixel intensity values from separate normoxic or hypoxic colonies. *P < .05, **P < .005, ***P < .001, ****P < .0001.

differentiate as they exit the cell cycle. Together, these findings demonstrate that over 24 hours of hypoxia, hISCs negatively regulate progression through the cell cycle and that hypoxia likely promotes G1 dormancy in hISCs.

Hypoxia Alters hISC Cell Cycle Regulation by Specific ILs

We next explored whether the hypoxia-regulated IL receptors could impact hISC cell cycle when in the presence of their cognate ILs: IL1a, IL1 β , IL2, IL4, IL6, IL10, IL13, IL17 (heterodimer), IL22, and IL25. hISC monolayers were treated with ILs under normoxia or hypoxia for 24 hours to simulate ILs that might be present during an chronic inflammatory response before fixing, staining, and

imaging. 8,12,71-74 No ILs caused significant impacts on the total proportion of proliferating cells (KI67⁺) after 24 hours of hypoxia; however, at 24 hours of normoxia or hypoxia, hISCs shift cell cycle phase dynamics in response to IL signals (Figure 7A-F). IL1a increases the proportion of hISCs in S-phase in normoxia, but this effect is largely abrogated in hypoxic hISCs (Figure 7A). IL2, IL4, and IL25 significantly increase the percentage of hISCs in M-phase only in hypoxia, with no change noted in normoxia (Figure 7B-E), whereas IL22 affects normoxic hISCs, but not hypoxic (Figure 7F). IL6, IL10, IL13, and IL17^{A/F} had no effects on cell cycle phase dynamics (Figure 8A-D). The IL1a-dependent decrease in S-phase cells with no increase in M-phase hISCs suggests that IL1a further promotes G1 arrest or elongation under hypoxia, thereby reducing

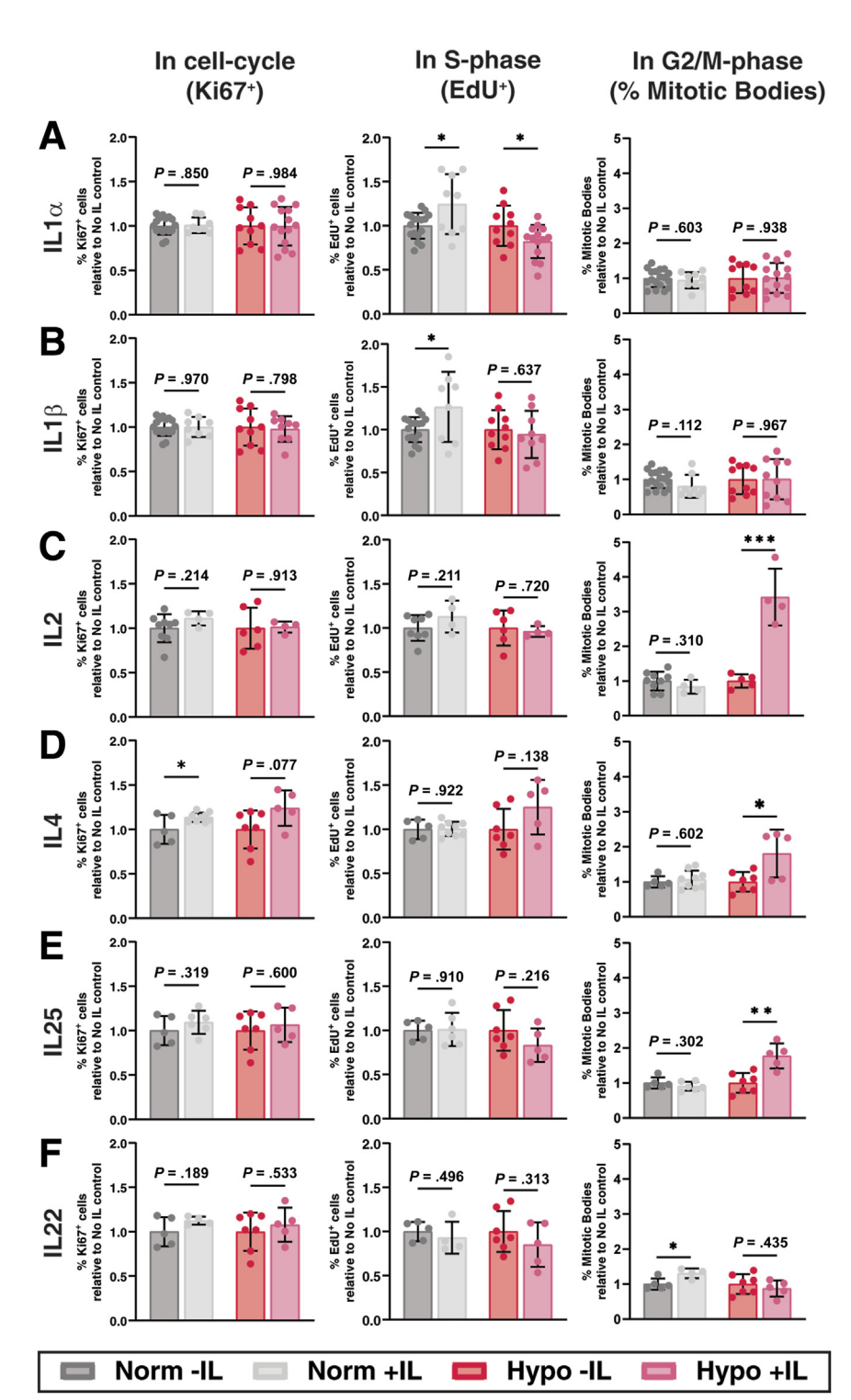


Figure 7. Hypoxia primes hISCs to respond to select ILs. (A) Quantification of cell cycle progression metrics from Figure 5E for hISCs treated with 24 hours of normoxia or hypoxia with or without IL1a. (B) Quantification of cell cycle progression metrics Figure 5E for hISCs treated with 24 hours of normoxia or hypoxia with or without IL1 β . (C) Quantification of cell progression metrics from Figure 5E for hISCs treated with 24 hours of normoxia or hypoxia with or without IL2. (D) Quantification of cell progression metrics cycle from Figure 5E for hISCs treated with 24 hours of normoxia or hypoxia with or without IL4. (E) Quantification of cell cvcle progression metrics from Figure 5E for hISCs treated with 24 hours of normoxia or hypoxia with or without IL25. (F) Quantification of cell cycle progression metrics from Figure 5E for hISCs treated with 24 hours of normoxia or hypoxia with or without IL22. * $P < .05, **\dot{P} < .005, ***P <$.001, ****P < .0001.

observable S-phase cells. IL2-, IL4-, and IL25-dependent increases in M-phase hISCs with no observable decrease in KI67 $^+$ cells suggest slow progression of hISCs through M-phase under hypoxic conditions. These indicate that hypoxia primes hISCs to respond to ILs differently then hISCs in normoxia

Hypoxia Affects hISC Activity in Response to IL Treatment

While the previous experiments were designed to focus on the impact of hypoxia-dependent IL receptor priming on proliferation dynamics, we next sought to probe whether this IL receptor priming would regulate stem cell activity in

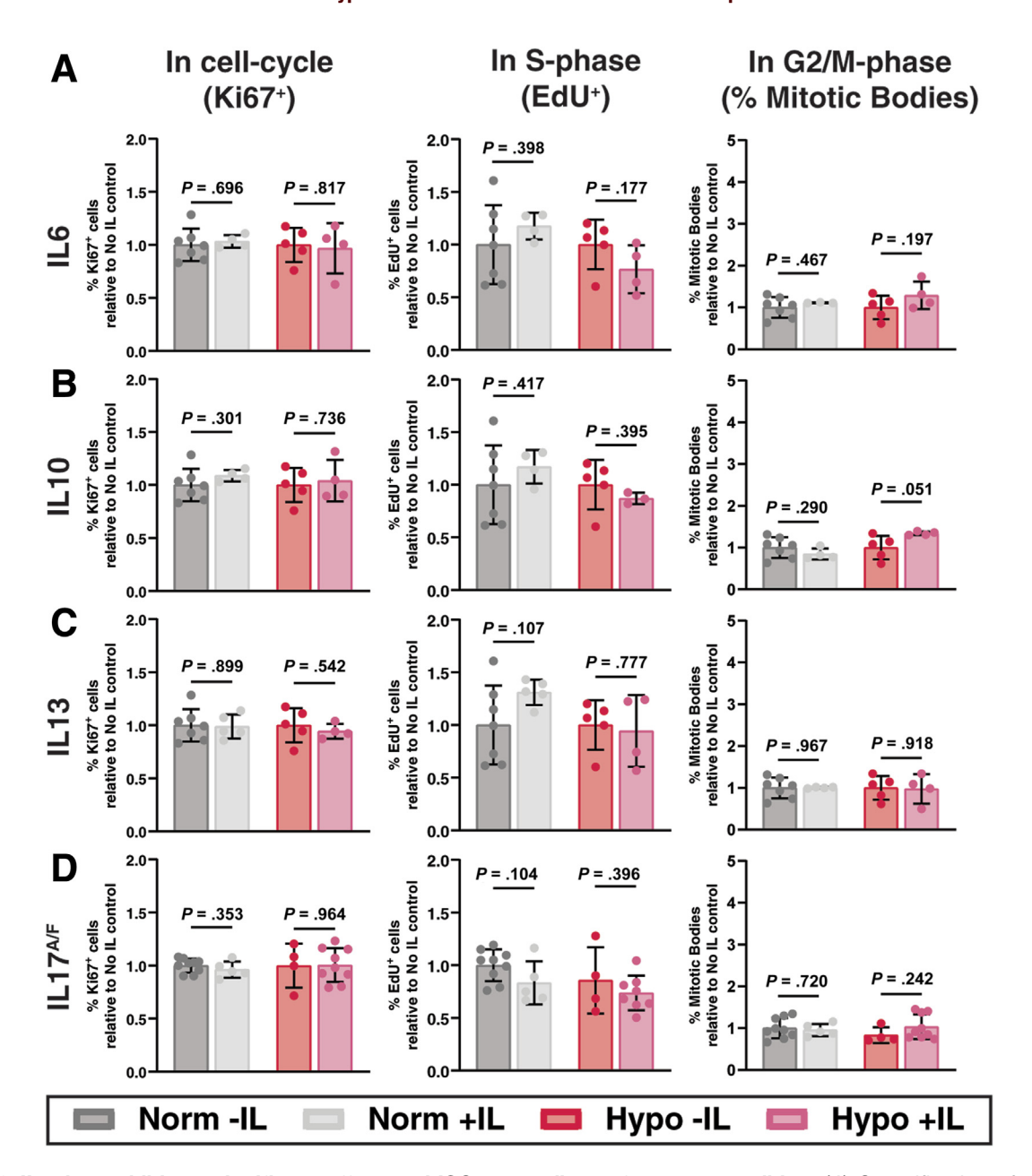


Figure 8. ILs that exhibit no significant effect on hISCs regardless of oxygen condition. (A) Quantification of cell cycle progression metrics from Figure 5E for hISCs treated with 24 hours of normoxia or hypoxia with or without IL6. (B) Quantification of cell cycle progression metrics from Figure 5E for hISCs treated with 24 hours of normoxia or hypoxia with or without IL10. (C) Quantification of cell cycle progression metrics from Figure 5E for hISCs treated with 24 hours of normoxia or hypoxia with or without IL13. (D) Quantification of cell cycle progression metrics from Figure 5E for hISCs treated with 24 hours of normoxia or hypoxia with or without IL17^{A/F}.

the presence of cognate ILs. hISC monolayers were exposed to 24 hours of normoxia or severe hypoxia, then dissociated to single hISCs and plated in conventional 3D organoid assays to evaluate OFE of clonal hISCs in the absence or presences of ILs (Figure 9A). Similar to OFE assays in the CRAs (Figure 2F), we found that hypoxia induced a decrease in OFE at 24 hours (Figure 9B and C). IL6, IL10, and IL13 (Figure 9D-F) increased OFE in a hypoxia-independent manner, while IL1 β , IL2, IL4, and IL25 demonstrated hypoxia-dependent increases in OFE (Figure 9G-J), thereby rescuing the negative impacts of hypoxia on hISC. No effects

on OFE were observed for IL1a, IL17^{A/F}, and IL22 (Figure 9*K*–*M*).Together, these findings show 24 hours of hypoxia primes hISCs to respond to cognate ILs differently in hypoxia than in normoxia by altering cell cycle phase dynamics and in some cases enhancing hISC activity.

Discussion

Human health conditions that cause loss of oxygen to the intestinal epithelium result in rapid loss of the differentiated cells, requiring quick regeneration from the stem cell pools

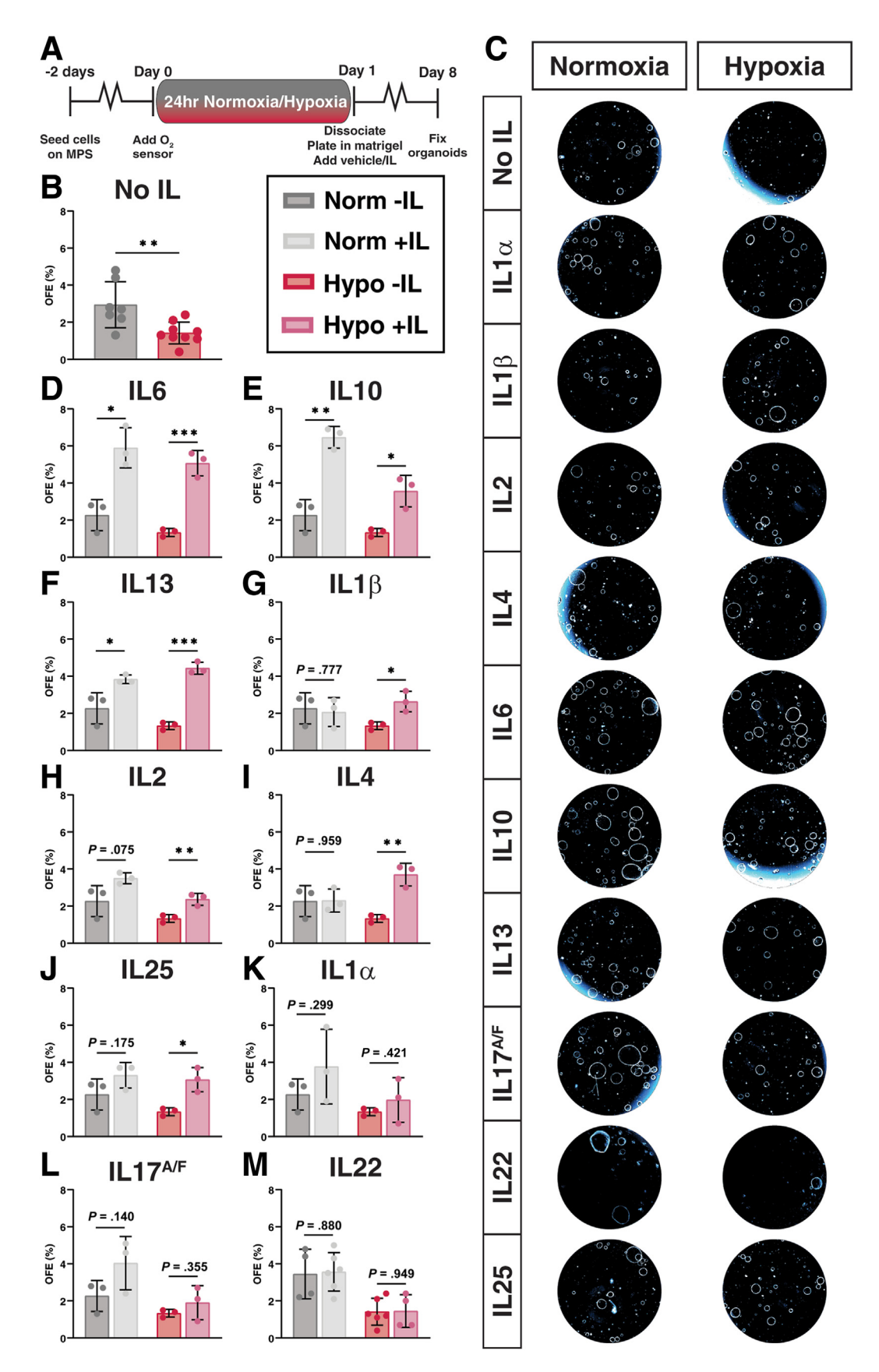


Figure 9. hISCs demonstrate hypoxia-dependent rescue of OFE when treated with specific ILs. (A) Experimental schematic to assess impact of hypoxia, then reoxygenation and ILs on functional stem cell activity. (B) Impact of hypoxia and reoxygenation on functional stem cell activity without treatment of ILs. (C) Representative images of organoids from conditions in panels B and D-M. Images have been pseudo-colored to highlight outer membranes of organoids. (D-M) Impact of hypoxia and reoxygenation plus ILs screened from Figures 7 and 8 on functional stem cell activity. Organoid formation efficiencies from corresponding normoxic and hypoxic no-IL and IL-treated samples were compared using unpaired t tests. *P < .05, **P < .005, ***P < .001, ****P < .0001.

located at the base of the crypts.^{6,75,76} Evaluating the impact of hypoxia on hISCs in vivo is challenging due to ethical considerations and the inability to precisely control many experimental variables. While in vitro systems are available to regulate ambient oxygen levels, these platforms are limited in that oxygen levels are monitored in large volume incubators and not localized to the cell-medium interface. Here, we developed a flexible and oxygen-tunable MPS that addresses many limitations of conventional systems and represents a next-generation platform to study hypoxic injury across a broad range of cell and tissue types. While not explored in this study, the flexible design and small scale of the MPS will enable coculture of hISC with other cell types, such as immune cells, which are key players in hypoxia-related intestinal conditions.

Murine intestinal epithelial monolayers were shown to experience repeated bouts of hypoxia during conventional cell culture methods.³⁸ Upon media changes, oxygen levels were at saturation but the levels substantially reduced in media over time, ostensibly by cellular metabolism, thereby creating a hypoxic environment and inducing a HIF1a response.³⁸ These observations indicate that oxygen diffusion from ambient incubator gas mixes was insufficient to compensate for the oxygen metabolism of mouse intestinal epithelial cells submerged in culture media.³⁸ Using our newly developed MPS that supports 2D cultures of hISCs, we show similar findings in that fresh media at the cell surface interface is saturated at about ~12% O2 from atmospheric gasses and that hISCs metabolize 02 levels in the media from $\sim 12\%$ to $\sim 3\%$ in approximately 3 hours. At that point, O2 levels stabilize but are sufficiently low to induce a small but appreciable hypoxia-induced HIF1a response after 24 hours of submersion culture. Our findings challenge general assumptions regarding oxygen availability following regular medium changes in many conventional cell culture systems. More specifically, our data suggest that any cells cultured in submersion culture can experience unappreciated HIF1a-dependent transcriptional changes following media changes, confounding interpretations.

Our findings show that hISCs are highly resilient to severe hypoxia for up to 48 hours. There was a decrease in functional hISC activity at 24 hours of hypoxia, but this resolved at 48 hours with no significant difference in OFE compared with normoxic controls. Several studies in rodent and human intestines highlight the role of endoplasmic reticulum stress and the unfolded protein response during acute hypoxic episodes. 38,77,78 The unfolded protein response is considered to mediate cell death by activating the intrinsic apoptotic cascade; however, several more contemporary reports in the context of cancer cell lines indicate that unresolved endoplasmic reticulum stress, which can occur during long durations of hypoxia,⁵² can induce necroptosis. 52,79,80 We found no clear evidence of increased apoptosis during 48 hours of severe hypoxia, and while necroptosis pathways were not evaluated, there was no decrease in hISC activity at 48 hours of hypoxia, strongly supporting that other cell death pathways are being repressed in hISCs through 48 hours of hypoxia.

Transcriptomic profiling of hISCs during chronic and severe hypoxia revealed enrichment of regulated genes related to inflammation and inflammation responses. Among these genes, we noticed many cytokine/IL receptors were significantly regulated in a hypoxia-dependent manner. While the IL responses mediated through these receptors impact many different aspects of cell biology, we focused our analysis on how hypoxia-induced changes in hISC expression of IL receptors could impact cell cycle dynamics and stem cell activity through stimulation using their cognate ILs. In the absence of ILs, the baseline hISC response to 24 hours of hypoxia was a significant decrease in the overall number of cycling cells (KI67⁺) with notable reductions in numbers of cells in each phase of the cell cycle. While the number of cycling cells was reduced at 24 hours of hypoxia based on KI67, the lack of differentiated cell markers and absence of reduced OFE of hISCs at 48 hours suggests that hISCs do not exit cell cycle or differentiate as the result of severe hypoxia but rather enter a safe mode characterized by a reversable dormant state, reminiscent of a reserve ISC state.⁸¹ Further genetic and molecular analysis will be necessary to reveal these mechanisms.

Pharmacologic manipulation to enhance HIF1a activity has demonstrated some protective effects (eg, increased barrier function, decreased apoptosis, decreased proinflammatory signaling) and stabilization of HIF-1 through inhibition of PHDs has been shown to also induce protective and regenerative effects in cell culture and animal models. 82-85 Our results demonstrate variable effects of different PHD inhibitors on primary hISCs. Roxadustat induces significant upregulation of HIF1a target genes, whereas DMOG does not. Furthermore, treatment of hISCs with Roxadustat for 24 hours does not induce the magnitude of IL receptor upregulation compared with 24 hours of hypoxia, suggesting that IL receptors may be regulated in part by HIFindependent mechanisms. Treatment of hypoxic hISCs with HIF1a inhibitors PX-478 and KC7F2 did not reduce gene expression of HIF target genes when hISCs were under hypoxia, suggesting that these drugs may not be viable candidates for inhibiting HIF in hISCs at the concentrations tested. The variable impact of these drugs on PHD and HIF1a inhibition in primary hISCs was not expected. Previous reports describe expression of ABC-transporters that efflux drugs in hISCs, which could explain the lack of hISC response to DMOG, PX-478, and KC7F2, despite use of the highest dose that did not produce toxicity.86 Furthermore, reports of additional regulatory pathways that control HIF target genes, such as activation of GLUT1 by AMPK instead of HIF1 demonstrate that inhibition of PHDs and HIF may not be sufficient to induce the full activation of some HIF target genes.87 This small drug screen highlights the utility of the microphysiological hypoxia system to test efficacy of drugs on hISCs.

During inflammatory hypoxia, local immune cells express a complex mixture of ILs near hISCs.⁸ In our model, hypoxia primed hISCs to respond to subsets of ILs by regulating cognate IL receptors. Stimulation of hypoxia-regulated IL receptors by their cognate ILs produced notable hypoxia-dependent increases in G2/M-phase cells

for IL2, IL4, and IL25 that generally rescued the baseline hypoxia-dependent loss of G2/M-phase cells. Less notable, IL1a caused a modest but significant reduction in S-phase cells. There is a collection of studies describing how IL2 and IL4 promote proliferation in immune cells, 55,58,88,89 and studies in colon and pancreatic cancer cells demonstrate that IL4 enhances proliferation, 90,91 but we found no studies describing the role of these ILs on mouse or human ISCs. IL25 is expressed by tuft cells during parasitic worm infections. Secreted IL25 interacts with the cognate heterodimer receptors, IL17RA and IL17RB, on innate lymphoid cells type 2, which signal back through IL-4 and IL-13 to the epithelium to aid worm clearance. 22,94,95,97 IL17RA/B expression has not previously been reported in hISCs, suggesting a novel role for IL25 signaling in hISCs.

Under 24 hours of hypoxia, hISCs demonstrate less active progression through the cell cycle and lower OFE. hISCs show increased stem cell activity in response to IL6, IL10, and IL13, regardless of hypoxic conditioning. On the other hand, hypoxia induces hISCs to respond to $IL1\beta$, IL2, IL4, and IL25 by increasing stem cell activity in a hypoxiadependent fashion. IL2 and IL4 promote cell survival effects by stimulating the Akt-pathway, 98 and although there are fewer clear links between IL25 (IL17RA/B) and cell survival, the IL17RA/B receptors can stimulate nuclear factor κB (NF- κB) activation, ^{99,100} which has cell survival effects under some stress stimuli. ¹⁰¹ While hypoxia alone can stimulate NF-κB activation through HIF1a,8,102 IL25 could amplify NF-kB activation to increase hISC survival during severe and prolonged hypoxic episodes. Interestingly, IL2, IL4, and IL25 stimulated increases in G2/M in hISCs under hypoxia, with no change seen in hISCs under normoxia. G2/M arrest or delay by these 3 cytokines might protect cells from undergoing checkpoint-induced cell death as the completion of cytokinesis could be compromised by the lack of energetic and metabolic resources under severe hypoxia. While many ILs have cell cycle effects on hISCs under normoxia, we see that many of these effects change and produce novel responses that are only seen in the context of hypoxia. As such, it appears hypoxia-primed hISCs likely respond differently to immune stimuli than normoxic hISCs, laying the foundation for studies into unique, hypoxia-dependent genetic and biochemical mechanisms, which preserve and restore hISC activity during and after hypoxic injury.

We acknowledge that deconstruction of the complex microenvironment of the in vivo human stem cell niche limits some physiological interpretations. However, second-generation studies using our MPS can build on the findings of this study to test complex mixtures of hypoxia-related cytokines, interactions of multiple cell types, and tunable O_2 concentrations to more accurately model and study hISC behaviors under inflammatory hypoxia, more acute forms of oxygen deprivation, and clinically relevant reperfusion. Previous iterations of the MPS have shown the ability of the MPS to dynamically reperfuse hypoxic cultures with O_2 , enabling studies of other modes cell death, such as ferroptosis, which likely have a role in reperfusion injury due to reactive oxygen species production, 26,104,105 or pyroptosis,

which are relevant to inflammasome-mediated cell death and are complex to model, as they involve microbes and immune cell components. As such the MPS is currently being optimized for coculture of hISCs, immune cells, and anaerobic commensal or pathological microbiota with the goal of creating a more physiologically relevant environment to explore many facets that impact hISC function and behavior.

Materials and Methods

Primary Human Crypt Isolation and Intestinal Epithelial Stem Cell Culture

A surgical specimen of human small intestine (jejunum) was obtained from a donor at UNC Hospitals with consent of the patient (under the approved protocol UNC IRB #14-2013). Villi and crypts were detached from the specimen by incubation in a chelating buffer for 75 minutes at 20°C followed by vigorous shaking in a 50 mL conical tube. The chelating buffer was composed of EDTA (2 mM), dithiothreitol (0.5 mM, freshly added), Na₂HPO₄ (5.6 mM), KH₂PO₄ (8.0 mM), NaCl (96.2 mM), KCl (1.6 mM), sucrose (43.4 mM), and D-sorbitol (54.9 mM), with pH 1/4 7.4. 108 Released crypts were expanded as a monolayer on a neutralized collagen hydrogel as described previously.²⁵ Briefly, crypts were placed on the top of 1.0 mg/mL collagen hydrogels (1 mL into each well of 6-well plate (T1006; Denville) at a density of 5,000 crypts/ well and overlaid with 4 mL of expansion media (EM) containing 10 mmol/L Y-27632 (S1049; Selleck Chemicals). EM contains a mixture of advanced Dulbecco's modified Eagle medium/ F12 medium (12634010; Thermo Fisher Scientific) and conditioned medium (WRN medium prepared in lab from L-WRN cells (CRL-3276; ATCC) following a published protocol¹⁰⁹ at a volumetric ratio of 1:1, and supplemented with GlutaMAX (35050061; Thermo Fisher Scientific), B27 supplement without vitamin A (12587010; Thermo Fisher Scientific), 10 mM HEPES (15630-080; Thermo Fisher Scientific), 1.25 mM N-acetyl cysteine (194603; MP Bio), 10 mM nicotinamide (N0636; Sigma-Aldrich), 50 ng/mL epidermal growth factor (315-09; PeproTech), 2.0 nM gastrin (AS-64149; Anaspec), 10 nM prostaglandin E2 (14010; Cayman Chemicals), 3.0 μ M SB202190 (S1077; Selleck Chemicals), 100 U/mL penicillin-streptomycin (15140122; Thermo Fisher Scientific), and 50 mg/mL primocin (ant-pm-1; InvivoGen). EM was used to expand the epithelial cell numbers as monolayers or organoids. Y-27632 was present only in the first 48 hours of cell culture and was not added to subsequent media changes. The medium was changed every 48 hours. When the cell coverage was greater than 80% (typically 5-7 days), the epithelium was dissociated to fragments to seed onto the intestinal MPS or passaged for further expansion.

Fabrication of Primary Human Intestinal MPS

The human intestinal MPS was fabricated from polymethylmethacrylate (PMMA) and photocured resin (Formlabs, Inc). PMMA provided an optically transparent material with a low oxygen diffusion coefficient that could

be sterilized and reused. 110 The photocured resin provided a 3D-printable bottom frame to support the PMMA device and simultaneously house the optical reader for oxygen measurements. The cell culture chamber and gas exchange channels were fabricated from 5.8-mm-thick and 1.5 mmthick PMMA sheets (44352, 44292; US Plastics). The microfluidic culture region was composed of 5 rectangular wells, with dimensions of 11.6 mm by 7.0 mm each. The rectangular gas channel on top of the wells was 70 mm by 45 mm by 1.5 mm. The bottom and top pieces of PMMA were laser cut from a 1.5-mm-thick PMMA sheet, while the middle piece, for the cell culture wells, was laser cut from a 5.8-mm-thick PMMA sheet. Briefly, to remove dust and burr material with minimal cracking, each PMMA surface was quickly wiped with 100% IPA solution and air-dried. All 3 pieces were pressed together between 2 sheets of brass using a pneumatic heat press (SwingPress 10-0403; Across International). Annealing was performed with the heat press set at 100°C and 300 psi for 2 hours, then the bonded device was cooled for 3 hours at room temperature. A rubber gasket was laser cut and placed on top of the PMMA layer to seal the device, prior to bolting together. The device was tested for leaks using red and blue dyed water and cracks were sealed by application of dichloromethane to the seams.

In the completed device, barbed connectors screwed into the photopolymer resin top lid provide gas flow into and out of the device. A rubber gasket seals gas flow into and out of the PMMA gas exchange channel. The gas exchange channel frame is bonded to the PMMA culture chamber and PMMA base support. A photopolymer resin bottom frame supports the entire PMMA device, and screws attach the top lid to the bottom frame to seal the MPS closed. The optics front-end connects via a μ USB-to-HDMI cord to a phosphorescence-lifetime fluorimeter detector and interrogates the middle culture well, where the iPOB is located.

A neutralized collagen hydrogel (2.0 mg/mL) was cast into each well of a prefabricated PMMA device and allowed to polymerize at $37^{\circ}\mathrm{C}$ for 1 hour. Then, 250 $\mu\mathrm{L}$ of 1X Dulbecco's phosphate-buffered saline (DPBS) was overlaid on the polymerized hydrogel and allowed to preswell for at least 5 hours at room temperature. DPBS was removed and the hydrogel was rinsed 3 times before overlaying with 250 $\mu\mathrm{L}$ of EM containing hISCs that had been mechanically dissociated by pipetting 10 times until cells were $\sim 1\text{--}10$ cell clumps. Once the hISCs formed a confluent monolayer, an iPOB was added to the epithelium to measure oxygen.

Real-Time Monitoring and Control of Oxygen Concentration in 2D Culture

Oxygen concentration in the system was continuously measured with an integrated phosphorescent oxygen sensor (iPOB) using NIR phosphorescence lifetime fluorimetry. The iPOB is composed of porous pHEMA gel functionalized with palladium-benzoporphyrin derivatives (Pd-BPD) that respond to local oxygen concentrations via phosphorescence quenching.²⁷ The photoluminescence excitation and detection wavelengths are 630 nm and 800 nm, respectively. The iPOB (Profusa) has been manufactured in a

variety of sizes, but for all experiments a disk-shaped, 5mm-diameter, 0.5-mm-thickness iPOB was used. The optics front end of the NIR phosphorescence lifetime fluoroscope (Profusa) was inserted into the support frame below the MPS. The oxygen concentration was controlled via a PMMA gas-mixing microfluidic chip with tubing connecting outlets from the gas-mixing chip to the inlets of each MPS (Figure 10A and B). The gas-mixing chip was previously used to generate 8 concentrations of mixed gas, ranging from less than 3 μM of oxygen to 180 μM . (Figure 10C and D)¹¹¹ Gas flow to the gas-mixing chip was regulated using an air flow control valve (62005K313; McMaster-Carr) and monitored with a mass flow meter with digital output (GFMS-010061; Aalborg GFM) (Figure 10B, left). Hydrated mixed gas exiting the gasmixing chip was introduced into individual MPS at a rate of 5 mL/min to prevent media evaporation. Within 30 minutes, the gas mixture equilibrated with the local MPS environment to generate the desired oxygen concentration at the hydrogel surface-media interface where oxygen was measured using the iPOB (Figure 1D). The intestinal epithelium inside MPS was cultured in the mixed gas environment and compared with intestinal epithelium statically cultured in a normobaric incubator with an oxygen environment of 186 μ M.

Immunofluorescence Staining

To assess the impact of various durations and magnitudes of hypoxia on hISC proliferation, primary human intestinal epithelium and single cells isolated from each MPS chamber were stained for KI67. For KI67 staining of intestinal epithelium following hypoxia, the intestinal MPS was opened, and media was removed from each chamber. Intestinal epithelium on top of the collagen hydrogels were fixed with 4% PFA for 15 minutes. After fixation, samples were rinsed once with 1X phosphate-buffered saline (PBS) and overlaid with PBS. Samples were permeabilized for 15 minutes with 0.5% Triton-X 100 in 1X PBS. Samples were blocked for 30 minutes with a 3% bovine serum albumin solution. After blocking, samples were stained for proliferation marker Ki-67 Alexa Fluor 647 (1:250 dilution in 3% bovine serum albumin, Cat. No. 652407; BioLegend) for 1 hour and nuclei counterstain bisbenzimide (1:1000 dilution in 1X DPBS, Cat. No. 1155; Millipore Sigma) for 5 minutes at room temperature. To look at cell-cell contacts, tight junction protein occludin (Cat. No. 13409-1-AP; Proteintech) was added for 1 hour, followed by incubator with the secondary antibody Cy3 (Cat. No. C2306; Sigma) for 2 hours. After staining, the gels were overlaid with 1X DPBS and stored at 4°C until imaging. Brightfield and fluorescent images were obtained with a Olympus IX81 microscope, using Metamorph Basic (Molecular Devices) software or a Keyence BZ-X800 fluorescent microscope using a $4\times/0.13$ Plan Fluorite Keyence or $10 \times /0.45$ Plan Apochromat Fluorite Keyence objective.

For quantifying cell cycle dynamics, a Zeiss LSM700 confocal microscope using a Plan-Apochromat $10\times/0.45$ M27 objective. Fluorescent image quantification and

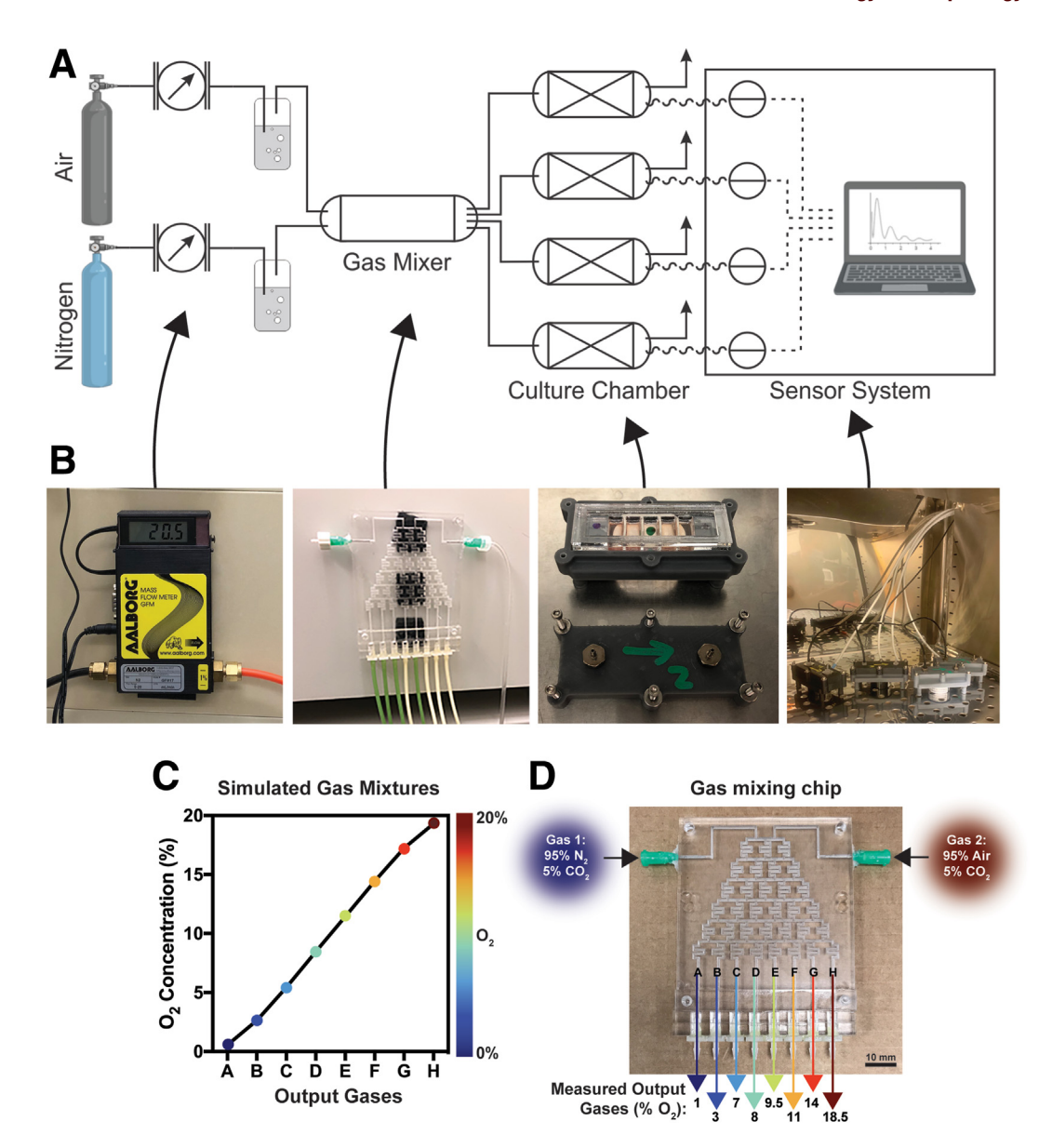


Figure 10. Gas mixing chip integrated into microphysiological system to generate 8 different oxygen environments. (A) Schematic of complete microphysiological system design with mixed gases in tanks leading into flow meters. Flow meters connect into humidification 15-mL conical tube filled with sterile PBS. Humidified gases travel into each input of the gas mixer chip, and 8 concentrations of gases exit individual outlets to connect into separate microphysiological systems (devices). Device oxygen concentration is monitored using detectors that send information to a laptop located beside the incubator. (B) Images taken of each component of the system. (C) COMSOL Multiphysics results for the simulated gas mixtures from each outlet of the gas mixing chip. (D) Image of the gas mixing chip and measured output oxygen concentrations recorded inside individual devices.

analysis was done using scikit-learn and ImageJ v1.53q (National Institutes of Health). 112,113

Drug Titrations and Treatment on Primary hISC Cultures

Four drugs were tested based on their potential to either stabilize HIF in normoxia—PHD inhibitors: Roxadustat (Selleck Chemicals; S1007) or DMOG (Selleck Chemicals; S7483)—or inhibit HIF in hypoxia—PX478 (Selleck Chemicals; S7612) or KC7F2 (Selleck Chemicals; S7946). To

determine concentrations of these drugs to use in experiments with primary cells we searched literature to determine a potential range. Then, primary human jejunum cells were incubated for 24 hours with these various concentrations (Table 1), then fixed and stained for KI67, DAPI, and CC3. The maximum concentrations that did not result in clear effects on cell proliferation or monolayer integrity were chosen for further experiments.

To perform drug screening experiments, primary human jejunum cells were passaged onto 2 mg collage as previously described, cultured to 30%–40% confluency, then treated

Table 1. Drug Concentrations Tested and Used in PHD and HIF Inhibitor Studies					
Drug	Class	Concentrations Tested	Concentration Used		
Roxadustat	PHD inhibitor	10 uM, 25 uM, 50 uM, 100 uM, 250 uM	250 uM		
DMOG	PHD inhibitor	10 uM, 50 uM, 100 uM, 500 uM, 1 mM	100 uM		
PX-478	HIF Inhibitor	5 uM, 10 uM, 15 uM, 20 uM, 25 uM	25 uM		
KC7F2 ^a	HIF Inhibitor	5 uM, 10 uM, 25 uM, 50 uM, 100 uM	25 uM		

DMOG, dimethyloxalylglycine; HIF, hypoxia-inducible factor; PHD, prolyl hydroxylase. ^aKC7F2 fell out of solution at concentrations above 25uM.

for 24 hours with amounts of drugs as determined above, in normoxia only for Roxadustat and DMOG, and in normoxia and hypoxia for PX-478 and KC7F2. After 24 hours of treatment, RNA was extracted, and quantitative real-time polymerase chain reaction (qRT-PCR) was performed for to evaluate expression of HIF1A target genes and IL receptors.

Single hISC-Derived OFE Assay

Following MPS culture, human intestinal epithelium was dissociated into single cells, sorted using a flow cytometer, and suspended in Matrigel on a quad CRA platform (Cell Microsystems).³³ Briefly, each sample was retrieved and placed in a separate conical. 500 U/mL Collagenase IV (17104019; Gibco) was added to breakdown the scaffold and incubated for 10 minutes at 37°C. After centrifugation, the cell pellet was rinsed twice in DPBS and resuspended in 150 μ L of 0.5 mmol/L EDTA in DPBS with 10 mmol/L Y-27632 and incubated for 5 minutes at 37°C. The fragments were further dispersed by triturating 30 times using a 200 μ L pipet tip. After centrifugation, the cell pellet was resuspended in 500 µL TrypLE Express (12605-036; Gibco) with 10 mmol/L Y-27632 and incubated for 5 minutes at 37°C. The cell suspension was gently triturated 7 times using a 28.5-gauge insulin needle to further dissociate. 500 μ L of EM was added to quench the reaction, and cells were pelleted and rinsed once in EM. After pelleting again, cells were resuspended in 200 μL of EM containing 1% fetal bovine serum. Immediately before FACS, APC Annexin V (1:200, 640941; BioLegend) was added to cells for live/dead

discrimination. After staining, cells were rinsed in EM and filtered through 0.4 μ m FACS tube top filter (352235; Corning). 5,000 Annexin V- live cells were isolated via FACS and resuspended in 250 µL of Growth Factor Reduced Matrigel (354230; Corning). Cell-gel suspensions were plated in each chamber of the quad CRA. To cover the CRA, each array was centrifuged at 200 g for 5 minutes. CRAs were polymerized for 20 minutes at 37°C in an incubator and then overlaid with EM containing 10 mmol/L Y-27632. Media was replaced every 2 days. To determine OFE, the CRA was scanned, and the total number of organoids was counted on day 2, day 4, and day 6. The OFE (%) was calculated as the total number of organoids created in 1 CRA chamber, divided by 5,000 cells and multiplied by 100. FACS and flow cytometry were performed using a SH800Z Cell Sorter (Sony Biotechnology, San Jose, CA).

IL Screen on Cell Cycle Phase Progression and Stem Cell Activity

Expansion wells of primary human monolayers were cultured in normal culture conditions until $\sim 80\%$ confluent and then dissociated and passaged onto MPS acrylic plates for exposure to normoxia (control) or hypoxia. After passaging onto acrylic plates, cells were cultured until $\sim 60\%$ confluent to maximize the number of individual stem-cell derived colonies and to limit contact-inhibition of hISC activity. To quantify the 5-ethynyl-2'-deoxyuridine (EdU) uptake using immunofluorescence staining under normoxia or hypoxia, various ILs were added before placing

Name	Stock Concentration	Working Concentration	Manufacturer	Cat #
IL1a	5 μg/mL	10 ng/mL	PeproTech	200-01A
IL1b	5 μ g/mL	10 ng/mL	PeproTech	200-01B
IL2	10 μg/mL	10 ng/mL	PeproTech	200-02
IL4	5 μ g/mL	20 ng/mL	PeproTech	200-04
IL6	100 μg/mL	10 ng/mL	R&D Systems	7270-IL-010
IL10	100 μg/mL	10 ng/mL	R&D Systems	217-IL0-010
IL13	5 μg/mL	20 ng/mL	PeproTech	200-13
IL17 ^{A/F}	100 μg/mL	100 ng/mL	BioLegend	580608
IL22	100 μg/mL	10 ng/mL	R&D Systems	782-IL-010
IL25	100 μg/mL	100 ng/mL	BioLegend	598902

hISC cultures under normoxic or hypoxic conditions. ILs were added at the concentrations shown in Table 2. During 24 hours of normoxia or hypoxia, hISC cultures were incubated with EdU (10 µM EdU; 900584; Sigma-Aldrich) following 22 hours of culture, then replaced into the respective normoxic or hypoxic environment, and then fixed with 37°C 4% PFA before staining for EdU. Fixed cells were then washed with and stored in DPBS before permeabilization and staining. Following permeabilization with 0.5% Triton X-100, cells were stained for EdU using EdU Reaction Buffer (4 mM CuSO₄, 2 µM sulfo-CY5-azide, 0.2 M ascorbic acid, in DPBS) for 1 hour at room temperature protected from light. A Whitley MG500 anaerobic workstation with an anaerobic mixed gas atmosphere $(N_2:H_2:CO_2 \rightarrow$ 80:10:10) was used to maintain hypoxic environments during experimental treatments of hypoxic hISCs.

To assess stem cell activity, hISCs monolayers were cultured in the same manner as previously described before passaging onto MPS acrylic plates and exposure to normoxia or hypoxia. After 24 hours of normoxia or hypoxia, hISCs were dissociated to single cells and plated in Matrigel at a concentration of 1000 single cells per 10 μ L patty with corresponding vehicle or IL treatment. Matrigel was supplemented with the same concentration of IL as described in Table 2. Organoid formation efficiency was evaluated after 6–8 days in culture and medium was changed every 2 days.

Flow Cytometry

Cells collected from normoxic and hypoxic MPS were dissociated following the protocol above up to the step of addition of TrypLE Express. Following trituration with the insulin needle and quenching with the EM, cells were pelleted and resuspended in 100 μ L of 1X DPBS. Approximately 50,000 cells from each chamber were fixed by adding 400 μL of 4% PFA solution while being constantly vortexed to prevent cell aggregation. After fixation, single cells were pelleted and resuspended in 0.3% Triton-X for 15 minutes to permeabilize the cell membrane. Single cells were pelleted and resuspended in a staining solution of DMEM containing 1% fetal bovine serum and anti-Ki-67 Alex Fluor 647 (1:250 dilution in 3% bovine serum albumin, Cat. No. 652407; BioLegend) for 1 hour on ice. After staining, cells were rinsed in PBS and filtered through 0.4 μm FACS tube top filter (352235; Corning). Ki-67-positive single cells were quantified by flow cytometry.

Quantitative RT-PCR

To assess the expression of genes that are responsive to hypoxia, human intestinal epithelial samples from each MPS were collected for qRT-PCR analysis. Briefly, cells attached to collagen hydrogels were lysed in 200 μ L of RNA Lysis buffer (AM1931; Thermo Fisher Scientific). Total RNA was extracted using RNAqueous-Micro Total RNA Isolation Kit (AM1931; Thermo Fisher Scientific) according to manufacturer's protocols. Complementary DNA was generated from $\sim\!2$ ng of total RNA from each sample using iScript Reverse Transcription Supermix for qRT-PCR (170-8891; Bio-Rad) according to manufacturer's protocols. cDNA was diluted

1:20 and 1 μ L was used for qRT-PCR using the following probes: $HIF1\alpha:Hs00153153_m1$, Hs00969289_m1, SLC2A1 (GLUT1): Hs00892681_m1, VEGFA: Hs00900055_m1, IL6R: Hs01075664_m1, IL10RB: Hs00175123_m1, IL17RB: Hs00218889_m1, IL22RA1: Hs00222035_m1 (Applied Biosystems), and SsoAdvanced Universal Probes Supermix (1725281; Bio-Rad) according to manufacturer's protocols, qRT-PCR was carried out in a StepOnePlus Real Time PCR System (Applied Biosystems). For each sample and experiment, triplicates were made and normalized to 18S messenger RNA levels. Fold change was expressed relative to normoxic controls using $\Delta\Delta$ CT analysis.¹¹⁴ All statistics for gene expression were generated using an unpaired Student's t test. In all statistical analysis, P < .05 was considered significant.

Bulk RNA Sequencing

To investigate the dynamic response of hISC to hypoxia at the whole transcriptomic level, we performed RNA sequencing on human intestinal epithelium exposed to 6, 24, or 48 hours of hypoxia inside intestinal MPS, along with normoxic control intestinal MPS, which were cultured for each respective time point with no hypoxia exposure. RNA samples were collected from each intestinal MPS, and Total RNA was extracted using RNAqueous-Micro Total RNA Isolation Kit (AM1931; Thermo Fisher Scientific) according to manufacturer's protocols and stored at -80° C. To assess RNA quality prior to submission for sequencing, an RNA integrity number was measured using the Agilent 2100 Bioanalyzer. After confirmation that each sample had an RNA integrity number of at least 8, integrated fluidic circuits for gene expression and genotyping analysis were prepared using the Advanta RNA-Seq NGS Library Prep Kit for the Fluidigm Juno.

Informatics

Gene level expression was obtained through pseudo alignment of reads to human genome GRCh38 using Kallisto. PC and sample correlation analysis were done with Bioconductor packages Biobase, cluster, and qvalue. Expression values for plotting were obtained by TMM normalization across all samples using EdgeR package and differential expression between normoxic and hypoxic samples at each time point was calculated from raw counts with DESeq2. Package and differential expression between normoxic and hypoxic samples at each time point was calculated from raw counts with DESeq2. Package and differential expression between normoxic and hypoxic samples at each time point was calculated from raw counts with DESeq2. Package and differential expression between normoxic and hypoxic samples at each time point was calculated from raw counts with DESeq2. Package and differential expression between normoxic and hypoxic samples at each time point was calculated from raw counts with DESeq2. Package and differential expression between normoxic and hypoxic samples at each time point was calculated from raw counts with DESeq2. Package and differential expression between normoxic and hypoxic samples at each time point was calculated from raw counts with DESeq2. Package and differential expression between normoxic and hypoxic samples at each time point was calculated from raw counts with DESeq2. Package and differential expression between normoxic and hypoxic samples are each time point was calculated from raw counts with DESeq2. Package and differential expression between normoxic and hypoxic samples are each time point was calculated from raw counts with DESeq2. Package and differential expression between normoxic and hypoxic samples from each duration of hypoxic samples

References

- Carreau A, El Hafny-Rahbi B, Matejuk A, et al. Why is the partial oxygen pressure of human tissues a crucial parameter? Small molecules and hypoxia. J Cell Mol Med 2011;15:1239–1253.
- Espey MG. Role of oxygen gradients in shaping redox relationships between the human intestine and its microbiota. Free Radical Biol Med 2013;55:130–140.

- 3. Zheng L, Kelly CJ, Colgan SP. Physiologic hypoxia and oxygen homeostasis in the healthy intestine. A review in the theme: cellular responses to hypoxia. Am J Physiol Cell Physiol 2015;309:C350–C360.
- Taylor CT, Colgan SP. Regulation of immunity and inflammation by hypoxia in immunological niches. Nat Rev Immunol 2017;17:774–785.
- Li G, Wang S, Fan Z. Oxidative stress in intestinal ischemia-reperfusion. Front Med (Lausanne) 2021;8: 750731.
- Gonzalez LM, Moeser AJ, Blikslager AT. Animal models of ischemia-reperfusion-induced intestinal injury: progress and promise for translational research. Am J Physiol Gastrointest Liver Physiol 2015;308:G63–G75.
- Saxena K, Jolly MK. Acute vs. chronic vs. cyclic hypoxia: their differential dynamics, molecular mechanisms, and effects on tumor progression. Biomolecules 2019;9:339.
- 8. Van Welden S, Selfridge AC, Hindryckx P. Intestinal hypoxia and hypoxia-induced signalling as therapeutic targets for IBD. Nat Rev Gastroenterol Hepatol 2017; 14:596–611.
- Shah YM. The role of hypoxia in intestinal inflammation.
 Mol Cell Pediatr 2016;3:1.
- Eltzschig HK, Carmeliet P. Hypoxia and inflammation. N Engl J Med 2011;364:656–665.
- 11. Campbell EL, Bruyninckx WJ, Kelly CJ, et al. Transmigrating neutrophils shape the mucosal microenvironment through localized oxygen depletion to influence resolution of inflammation. Immunity 2014;40:66–77.
- Eltzschig HK, Bratton DL, Colgan SP. Targeting hypoxia signalling for the treatment of ischaemic and inflammatory diseases. Nat Rev Drug Discov 2014; 13:852–869.
- Colgan SP, Furuta GT, Taylor CT. Hypoxia and innate immunity: keeping up with the HIFsters. Ann Rev Immunol 2020;38:341–363.
- Colgan SP, Taylor CT. Hypoxia: an alarm signal during intestinal inflammation. Nat Rev Gastroenterol Hepatol 2010;7:281–287.
- Guan Y, Worrell RT, Pritts TA, et al. Intestinal ischemiareperfusion injury: reversible and irreversible damage imaged in vivo. Am J Physiol Gastrointest Liver Physiol 2009;297:G187–G196.
- **16.** Cartwright IM, Colgan SP. The hypoxic tissue microenvironment as a driver of mucosal inflammatory resolution. Front Immunol 2023;14:1124774.
- 17. Blikslager AT, Roberts MC, Rhoads JM, et al. Is reperfusion injury an important cause of mucosal damage after porcine intestinal ischemia? Surgery 1997; 121:526–534.
- 18. Blikslager AT, Roberts MC, Rhoads JM, et al. Prostaglandins I2 and E2 have a synergistic role in rescuing epithelial barrier function in porcine ileum. J Clin Invest 1997;100:1928–1933.
- 19. Leenarts CA, Grootjans J, Hundscheid IH, et al. Histopathology of human small intestinal and colonic ischemia-reperfusion: experiences from human IRmodels. Histol Histopathol 2019;34:711–722.
- 20. Grootjans J, Lenaerts K, Derikx JPM, et al. Human intestinal ischemia-reperfusion-induced inflammation

- characterized: experiences from a new translational model. Am J Pathol 2010;176:2283–2291.
- Hundscheid IH, Grootjans J, Lenaerts K, et al. The human colon is more resistant to ischemia–reperfusion–induced tissue damage than the small intestine. Ann Surg 2015; 262:304–311.
- 22. Gonzalez LM, Stewart AS, Freund J, et al. Preservation of reserve intestinal epithelial stem cells following severe ischemic injury. Am J Physiol Gastrointest Liver Physiol 2019:316:G482–G494.
- 23. Singleton DC, Macann A, Wilson WR. Therapeutic targeting of the hypoxic tumour microenvironment. Nat Rev Clin Oncol 2021;18:751–772.
- 24. Derikx JPM, Matthijsen RA, de Bruïne AP, et al. Rapid reversal of human intestinal ischemia-reperfusion induced damage by shedding of injured enterocytes and reepithelialisation. PLoS One 2008;3:e3428.
- 25. Wang Y, DiSalvo D, Gunasekara DB, et al. Self-renewing monolayer of primary colonic or rectal epithelial cells. Cell Mol Gastroenterol Hepatol 2017;4:165–182.e7.
- 26. Rivera KR, Pozdin VA, Young AT, et al. Integrated phosphorescence-based photonic biosensor (iPOB) for monitoring oxygen levels in 3D cell culture systems. Biosens Bioelectron 2019;123:131–140.
- 27. Wisniewski NA, Nichols SP, Gamsey SJ, et al. Tissue-integrating oxygen sensors: continuous tracking of tissue hypoxia. Adv Exp Med Biol 2017;977:377–383.
- 28. Hinman SS, Wang Y, Kim R, et al. In vitro generation of self-renewing human intestinal epithelia over planar and shaped collagen hydrogels. Nat Protoc 2021; 16:352–382.
- 29. Formeister EJ, Sionas AL, Lorance DK, et al. Distinct SOX9 levels differentially mark stem/progenitor populations and enteroendocrine cells of the small intestine epithelium. Am J Physiol Gastrointest Liver Physiol 2009; 296:G1108–G1118.
- 30. Gracz AD, Ramalingam S, Magness ST. Sox9 expression marks a subset of CD24-expressing small intestine epithelial stem cells that form organoids in vitro. Am J Physiol Gastrointest Liver Physiol 2010;298:G590–G600.
- 31. Sato T, Clevers H. Growing self-organizing mini-guts from a single intestinal stem cell: mechanism and applications. Science 2013;340:1190–1194.
- 32. Wang Y, Ahmad AA, Shah PK, et al. Capture and 3D culture of colonic crypts and colonoids in a microarray platform. Lab Chip 2013;13:4625–4634.
- 33. Gracz AD, Williamson IA, Roche KC, et al. A high-throughput platform for stem cell niche cocultures and downstream gene expression analysis. Nat Cell Biol 2015;17:340–349.
- 34. Gjorevski N, Sachs N, Manfrin A, et al. Designer matrices for intestinal stem cell and organoid culture. Nature 2016;539:560–564.
- 35. Ebbesen P, Pettersen EO, Denekamp J, et al. Hypoxia, normoxia and hyperoxia: terminology for medical in vitro cell biology. Acta Oncol 2000;39:247–248.
- **36.** Taylor CT, Colgan SP. Hypoxia and gastrointestinal disease. J Mol Med 2007;85:1295–1300.
- 37. Semenza GL. HIF-1, O2, and the 3 PHDs. Cell 2001; 107:1–3.

Rivera et al

- 38. Wang Y, Chiang I-L, Ohara TE, et al. Long-term culture captures injury-repair cycles of colonic stem cells. Cell 2019;179:1144-1159.e15.
- 39. Huang LE, Arany Z, Livingston DM, et al. Activation of hypoxia-inducible transcription factor depends primarily upon redox-sensitive stabilization of its α subunit. J Biol Chem 1996;271:32253-32259.
- 40. Gradin K, McGuire J, Wenger RH, et al. Functional interference between hypoxia and dioxin signal transduction pathways: competition for recruitment of the Arnt transcription factor. Mol Cell Biol 1996;16:5221-5231.
- 41. Forsythe JA, Jiang BH, Iyer NV, et al. Activation of vascular endothelial growth factor gene transcription by hypoxia-inducible factor 1. Mol Cell Biol 1996; 16:4604-4613.
- 42. Ebert BL, Firth JD, Ratcliffe PJ. Hypoxia and mitochondrial inhibitors regulate expression of glucose transporter-1 via distinct Cis-acting sequences. Journal of Biological Chemistry 1995;270:29083-29089.
- 43. Kothari S, Cizeau J, McMillan-Ward E, et al. BNIP3 plays a role in hypoxic cell death in human epithelial cells that is inhibited by growth factors EGF and IGF. Oncogene 2003;22:4734-4744.
- 44. Koopman G, Reutlelingsperger CP, Kuijten GA, et al. Annexin V for flow cytometric detection of phosphatidylserine expression on B cells undergoing apoptosis. Blood 1994;84:1415-1420.
- 45. Stern A, Thompson B, Williams K, et al. The CellRaft AIR® system: a novel system enabling organoid imaging, identification, and isolation. SLAS Discov 2022;27:201-208.
- 46. Breau KA, Ok MT, Gomez-Martinez I, et al. Efficient transgenesis and homology-directed gene targeting in monolayers of primary human small intestinal and colonic epithelial stem cells. Stem Cell Rep 2022;17:1493-1506.
- 47. Burclaff J, Bliton RJ, Breau KA, et al. A proximal-to-distal survey of healthy adult human small intestine and colon epithelium by single-cell transcriptomics. Cell Mol Gastroenterol Hepatol 2022;13:1554-1589.
- 48. Carbon S, Ireland IA, Mungall CJ, et al. AmiGO: online access to ontology and annotation data. Bioinformatics 2009;25:288-289.
- 49. Hung J-H, Yang T-H, Hu Z, et al. Gene set enrichment analysis: performance evaluation and usage guidelines. Brief Bioinform 2012;13:281-291.
- 50. Kierans SJ, Taylor CT. Regulation of glycolysis by the hypoxia-inducible factor (HIF): implications for cellular physiology. J Physiol 2021;599:23-37.
- 51. Pugh CW, Ratcliffe PJ. Regulation of angiogenesis by hypoxia: role of the HIF system. Nat Med 2003;
- 52. Bartoszewska S, Collawn JF. Unfolded protein response (UPR) integrated signaling networks determine cell fate during hypoxia. Cell Mol Biol Lett 2020;
- 53. Benczik M, Gaffen SL. The interleukin (IL)-2 family cytokines: survival and proliferation signaling pathways in T lymphocytes. Immunol Invest 2004;33:109-142.
- 54. Bersudsky M, Lutski L, Fishman D, et al. Non-redundant properties of IL-1alpha and IL-1beta during acute colon inflammation in mice. Gut 2014;63:598-609.

- 55. Bischoff SC, Sellge G, Lorentz A, et al. IL-4 enhances proliferation and mediator release in mature human mast cells. Proc Natl Acad Sci U S A 1999;96:8080-8085.
- 56. Chen J, Wang Y, Shen L, et al. Could IL-25 be a potential therapeutic target for intestinal inflammatory diseases? Cytokine Growth Factor Rev 2023;69:43-50.
- 57. Dorronsoro A, Lang V, Ferrin I, et al. Intracellular role of IL-6 in mesenchymal stromal cell immunosuppression and proliferation. Sci Rep 2020;10:21853.
- 58. Jenkins SJ, Ruckerl D, Thomas GD, et al. IL-4 directly signals tissue-resident macrophages to proliferate beyond homeostatic levels controlled by CSF-1. J Exp Med 2013;210:2477-2491.
- 59. Junttila IS. Tuning the cytokine responses: an update on interleukin (IL)-4 and IL-13 receptor complexes. Front Immunol 2018;9:888.
- 60. Friedrich M, Pohin M, Powrie F. Cytokine networks in the pathophysiology of inflammatory bowel disease. Immunity 2019;50:992-1006.
- 61. Andrews C, McLean MH, Durum SK. Cytokine tuning of intestinal epithelial function. Front Immunol 2018;9:1270.
- 62. Neurath MF. Cytokines in inflammatory bowel disease. Nat Rev Immunol 2014;14:329-342.
- 63. Gomez-Martinez I, Bliton RJ, Breau KA, et al. A planar culture model of human absorptive enterocytes reveals metformin increases fatty acid oxidation and export. Cell Mol Gastroenterol Hepatol 2022;14:409-434.
- 64. Koh MY, Spivak-Kroizman T, Venturini S, et al. Molecular mechanisms for the activity of PX-478:an antitumor inhibitor of the hypoxia-inducible factor-1alpha. Mol Cancer Ther 2008;7:90–100.
- 65. Narita T, Yin S, Gelin CF, et al. Identification of a novel small molecule HIF-1alpha translation inhibitor. Clin Cancer Res 2009;15:6128-6136.
- 66. Ma S, Zhao Y, Lee WC, et al. Hypoxia induces HIF1 α dependent epigenetic vulnerability in triple negative breast cancer to confer immune effector dysfunction and resistance to anti-PD-1 immunotherapy. Nat Commun 2022;13:4118.
- 67. Zhu Y, Zhang Y, Zhao F, et al. Inhibition of HIF-1 α by PX-478 suppresses tumor growth of esophageal squamous cell cancer in vitro and in vivo. Am J Cancer Res 2017; 7:1198-1212.
- 68. Pachitariu M, Stringer C. Cellpose 2.0: how to train your own model. Nat Methods 2022;19:1634-1641.
- 69. Stringer C, Wang T, Michaelos M, et al. Cellpose: a generalist algorithm for cellular segmentation. Nat Methods 2021;18:100-106.
- 70. Miller I, Min M, Yang C, et al. Ki67 is a graded rather than a binary marker of proliferation vs quiescence. Cell Rep 2018;24:1105-1112.e5.
- 71. Malkov MI, Lee CT, Taylor CT. Regulation of the hypoxia-inducible factor (HIF) by pro-inflammatory cytokines. Cells 2021;10:2340.
- 72. Mao Y-M, Zhao C-N, Leng J, et al. Interleukin-13: a promising therapeutic target for autoimmune disease. Cytokine Growth Factor Rev 2019;45:9-23.
- 73. McLean MH, Neurath MF, Durum SK. Targeting interleukins for the treatment of inflammatory bowel disease-what lies beyond anti-TNF therapy? Inflamm Bowel Dis 2014;20:389-397.

- Li LJ, Gong C, Zhao MH, et al. Role of interleukin-22 in inflammatory bowel disease. World J Gastroenterol 2014;20:18177–18188.
- 75. Ziegler AL, Pridgen TA, Mills JK, et al. Epithelial restitution defect in neonatal jejunum is rescued by juvenile mucosal homogenate in a pig model of intestinal ischemic injury and repair. PLoS One 2018;13:e0200674.
- 76. Ziegler A, Gonzalez L, Blikslager A. Large animal models: the key to translational discovery in digestive disease research. Cell Mol Gastroenterol Hepatol 2016;2:716–724.
- 77. Grootjans J, Hodin CM, de Haan J-J, et al. Level of activation of the unfolded protein response correlates with Paneth cell apoptosis in human small intestine exposed to ischemia/ reperfusion. Gastroenterology 2011;140:529–539.e3.
- 78. Kip AM, Grootjans J, Manca M, et al. Temporal transcript profiling identifies a role for unfolded protein stress in human gut ischemia-reperfusion injury. Cell Mol Gastroenterol Hepatol 2022;13:681–694.
- Livezey M, Huang R, Hergenrother PJ, et al. Strong and sustained activation of the anticipatory unfolded protein response induces necrotic cell death. Cell Death Differ 2018;25:1796–1807.
- 80. Saveljeva S, Mc Laughlin SL, Vandenabeele P, et al. Endoplasmic reticulum stress induces ligandindependent TNFR1-mediated necroptosis in L929 cells. Cell Death Dis 2015;6:e1587.
- Bankaitis ED, Ha A, Kuo CJ, et al. Reserve stem cells in intestinal homeostasis and injury. Gastroenterology 2018;155:1348–1361.
- 82. Cummins EP, Seeballuck F, Keely SJ, et al. The hydroxylase inhibitor dimethyloxalylglycine is protective in a murine model of colitis. Gastroenterology 2008;134:156–165.
- 83. Tambuwala MM, Cummins EP, Lenihan CR, et al. Loss of prolyl hydroxylase-1 protects against colitis through reduced epithelial cell apoptosis and increased barrier function. Gastroenterology 2010;139:2093–2101.
- 84. Tambuwala MM, Manresa MC, Cummins EP, et al. Targeted delivery of the hydroxylase inhibitor DMOG provides enhanced efficacy with reduced systemic exposure in a murine model of colitis. J Control Release 2015;217:221–227.
- **85.** Feng Z, Cheng Y, Wang Y, et al. Roxadustat protect mice from DSS-induced colitis in vivo by up-regulation of TLR4. Genomics 2023;115:110585.
- 86. Emran TB, Shahriar A, Mahmud AR, et al. Multidrug resistance in cancer: understanding molecular mechanisms, immunoprevention and therapeutic approaches. Front Oncol 2022;12:891652.
- 87. Dengler F, Gäbel G. The fast lane of hypoxic adaptation: glucose transport is modulated via a HIF-hydroxylase-AMPK-axis in jejunum epithelium. Int J Mol Sci 2019; 20:4993
- 88. Moriggl R, Topham DJ, Teglund S, et al. Stat5 is required for IL-2-induced cell cycle progression of peripheral T cells. Immunity 1999;10:249–259.
- 89. Vella AT, Dow S, Potter TA, et al. Cytokine-induced survival of activated T cells in vitro and in vivo. Proc Natl Acad Sci U S A 1998;95:3810–3815.
- 90. Prokopchuk O, Liu Y, Henne-Bruns D, et al. Interleukin-4 enhances proliferation of human pancreatic cancer cells:

- evidence for autocrine and paracrine actions. Br J Cancer 2005;92:921–928.
- Koller FL, Hwang DG, Dozier EA, et al. Epithelial interleukin-4 receptor expression promotes colon tumor growth. Carcinogenesis 2010;31:1010–1017.
- 92. Gerbe F, Sidot E, Smyth DJ, et al. Intestinal epithelial tuft cells initiate type 2 mucosal immunity to helminth parasites. Nature 2016;529:226–230.
- 93. Gerbe F, Legraverend C, Jay P. The intestinal epithelium tuft cells: specification and function. Cell Mol Life Sci 2012;69:2907–2917.
- 94. von Moltke J, Ji M, Liang H-E, et al. Tuft-cell-derived IL-25 regulates an intestinal ILC2-epithelial response circuit. Nature 2016;529:221–225.
- 95. Howitt MR, Lavoie S, Michaud M, et al. Tuft cells, tastechemosensory cells, orchestrate parasite type 2 immunity in the gut. Science 2016;351:1329–1333.
- 96. Rickel EA, Siegel LA, Yoon B-RP, et al. Identification of functional roles for both IL-17RB and IL-17RA in mediating IL-25-induced activities. J Immunol 2008;181:4299–4310.
- **97.** Smith KA, Löser S, Varyani F, et al. Concerted IL-25R and IL-4Rα signaling drive innate type 2 effector immunity for optimal helminth expulsion. Elife 2018;7:e38269.
- 98. Lindemann MJ, Benczik M, Gaffen SL. Anti-apoptotic signaling by the interleukin-2 receptor reveals a function for cytoplasmic tyrosine residues within the common gamma (gamma c) receptor subunit. J Biol Chem 2003; 278:10239–10249.
- 99. Awane M, Andres PG, Li DJ, et al. NF-kappa B-inducing kinase is a common mediator of IL-17-, TNF-alpha-, and IL-1 beta-induced chemokine promoter activation in intestinal epithelial cells. J Immunol 1999;162:5337–5344.
- 100. Chang SH, Park H, Dong C. Act1 adaptor protein is an immediate and essential signaling component of interleukin-17 receptor. J Biol Chem 2006;281:35603–35607.
- 101. Yang CH, Murti A, Pfeffer SR, et al. IFNalpha/beta promotes cell survival by activating NF-kappa B. Proc Natl Acad Sci U S A 2000;97:13631–13636.
- 102. D'Ignazio L, Rocha S. Hypoxia Induced NF- κ B. Cells 2016;5:10.
- 103. Hasvold G, Lund-Andersen C, Lando M, et al. Hypoxiainduced alterations of G2 checkpoint regulators. Mol Oncol 2016;10:764–773.
- 104. Chen Y, Fan H, Wang S, et al. Ferroptosis: a novel therapeutic target for ischemia-reperfusion injury. Front Cell Dev Biol 2021;9:688605.
- 105. Li Y, Feng D, Wang Z, et al. Ischemia-induced ACSL4 activation contributes to ferroptosis-mediated tissue injury in intestinal ischemia/reperfusion. Cell Death Differ 2019;26:2284–2299.
- 106. Bergsbaken T, Fink SL, Cookson BT. Pyroptosis: host cell death and inflammation. Nat Rev Microbiol 2009; 7:99–109.
- 107. Wu Y, Zhang J, Yu S, et al. Cell pyroptosis in health and inflammatory diseases. Cell Death Discov 2022; 8:191.
- 108. Sato T, Stange DE, Ferrante M, et al. Long-term expansion of epithelial organoids from human colon, adenoma, adenocarcinoma, and Barrett's epithelium. Gastroenterology 2011;141:1762–1772.

- 109. Miyoshi H, Stappenbeck TS. In vitro expansion and genetic modification of gastrointestinal stem cells in spheroid culture. Nat Protoc 2013;8:2471–2482.
- 110. Rivera KR, Yokus MA, Erb PD, et al. Measuring and regulating oxygen levels in microphysiological systems: design, material, and sensor considerations. Analyst 2019;144:3190–3215.
- 111. Yao M, Sattler T, Rabbani ZN, et al. Mixing and delivery of multiple controlled oxygen environments to a single multiwell culture plate. Am J Physiol Cell Physiol 2018; 315:C766–C775.
- 112. Pedregosa F, Varoquaux G, Gramfort A, et al. Scikit-learn: machine learning in Python. J Mach Learn Res 2011;12:2825–2830.
- 113. Schindelin J, Arganda-Carreras I, Frise E, et al. Fiji: an open-source platform for biological-image analysis. Nat Methods 2012;9:676–682.
- 114. Livak KJ, Schmittgen TD. Analysis of relative gene expression data using real-time quantitative PCR and the $2-\Delta\Delta$ CT method. Methods 2001;25:402–408.
- 115. Bray NL, Pimentel H, Melsted P, et al. Near-optimal probabilistic RNA-seq quantification. Nat Biotechnol 2016;34:525–527.
- 116. Huber W, Carey VJ, Gentleman R, et al. Orchestrating high-throughput genomic analysis with Bioconductor. Nat Methods 2015;12:115–121.
- 117. Love MI, Huber W, Anders S. Moderated estimation of fold change and dispersion for RNA-seq data with DESeq2. Genome Biol 2014;15:550.
- 118. Robinson MD, McCarthy DJ, Smyth GK. edgeR: a bioconductor package for differential expression analysis of digital gene expression data. Bioinformatics 2010; 26:139–140.
- 119. Mootha VK, Lindgren CM, Eriksson K-F, et al. PGC-1alpha-responsive genes involved in oxidative phosphorylation are coordinately downregulated in human diabetes. Nat Genet 2003;34:267–273.
- 120. Subramanian A, Tamayo P, Mootha VK, et al. Gene set enrichment analysis: a knowledge-based approach for interpreting genome-wide expression profiles. Proc Natl Acad Sci U S A 2005;102:15545–15550.

Received February 13, 2023. Accepted July 27, 2023.

Correspondence

Address correspondence to: Scott T. Magness, PhD, University of North Carolina at Chapel Hill, 111 Mason Farm Rd. Rm. 4337 MBRB, CB#7032, Chapel Hill, North Carolina, 27599. e-mail: magness@med.unc.edu.

Acknowledgments

The authors thank all the members of the Magness Laboratory, specifically Dr Meryem Ok, and the Biointerface Lab, along with Drs Michael Gamcsik and Bailey Zwarycz for helpful discussions. The authors thank Gabrielle Cannon at the Advanced Analytics core at UNC Chapel Hill. The authors thank the Center for Gastrointestinal Biology and Disease. Sequencing datasets are available on the National Center for Biotechnology Information Gene Expression Omnibus under accession number GSE224973.

CRediT Authorship Contributions

Kristina R Rivera, PhD (Conceptualization: Lead; Data curation: Lead; Formal analysis: Lead; Funding acquisition: Supporting; Investigation: Lead; Methodology: Lead; Visualization: Lead; Writing – original draft: Lead; Writing – review & editing: Lead)

R. Jarrett Bliton, PhD (Conceptualization: Supporting; Data curation: Lead; Formal analysis: Lead; Investigation: Supporting; Methodology: Supporting; Software: Lead; Visualization: Lead; Writing – original draft: Supporting; Writing – review & editing: Lead)

Joseph Burclaff, PhD (Conceptualization: Supporting; Data curation: Supporting; Funding acquisition: Supporting; Methodology: Supporting; Visualization: Supporting; Writing – original draft: Supporting; Writing – review & editing: Supporting)

Michael J Czerwinski, PhD (Conceptualization: Supporting; Formal analysis: Supporting; Methodology: Supporting; Software: Supporting; Visualization: Supporting; Writing – original draft: Supporting)

Jintong Liu, BS (Data curation: Supporting; Investigation: Supporting)

Jessica M Trueblood, BS (Data curation: Supporting)

Caroline M Hinesley, BS (Data curation: Supporting)

Keith A Breau, BS (Formal analysis: Supporting; Software: Supporting; Visualization: Supporting; Writing – review & editing: Supporting)

Halston E. Deal, PhD (Methodology: Supporting; Project administration: Supporting; Resources: Supporting)

Shlok Joshi, BS (Data curation: Supporting)

Vladimir A. Pozdin, PhD (Resources: Supporting),

Ming Yao, PhD (Resources: Supporting)

Amanda Ziegler, DVM, PhD (Formal analysis: Supporting; Software: Supporting; Writing – review & editing: Supporting)

Anthony T Blikslager, DVM, PhD (Conceptualization: Supporting; Writing – review & editing: Supporting)

Michael A Daniele, PhD (Conceptualization: Lead; Funding acquisition: Lead; Methodology: Supporting; Project administration: Lead; Resources: Lead; Supervision: Lead; Writing – original draft: Lead; Writing – review & editing: Supporting)

Scott T Magness, PhD (Conceptualization: Lead; Funding acquisition: Lead; Methodology: Supporting; Resources: Lead; Supervision: Lead; Writing – original draft: Lead; Writing – review & editing: Lead)

Conflicts of Interest

This author discloses the following: Scott T. Magness owns a financial interest in Altis Biosystems, Inc. The remaining authors disclose no conflicts.

Funding

This work was supported by the Center for Gastrointestinal Biology and Disease (CGIBD) Advanced Analytics Core under National Institutes of Health grant P30 DK034987. This work was funded by the National Science Foundation, National Science Foundation (EEC-1160483), the Nanosystems Engineering Research Center for Advanced Self-Powered Systems of Integrated Sensors and Technologies (CCSS-1846911 [Michael A. Daniele] and CBE/EBS-2033997 [Michael A. Daniele, Scott T. Magness]). This work was supported by the National Institutes of Health under award number F32DK124929 F31DK118859 Rivera), (Kristina (Joseph Burclaff). R01DK109559 (Scott T. Magness), the Howard Hughes Medical Institute Gilliam Fellowship (Kristina Rivera), the Katherine E. Bullard Charitable Trust for Gastrointestinal Stem Cell and Regenerative Research (Scott T. Magness), and CGIBD Pilot & Feasibility Award P30 DK034987 (Michael A. Daniele/Scott T. Magness).